The Relevance of Contact Terms Versus Pion-Exchange Contributions in the Chiral Effective Field Theory Description of Nucleon-Nucleon Scattering

A Dissertation

Presented in Partial Fulfilment of the Requirements for the

Degree of Doctor of Philosophy

with a

Major in Physics

in the

College of Graduate Studies

University of Idaho

by

Hamdah Alanazi

Major Professor: Ruprecht Machleidt, Ph.D.

Committee Members: Francesca Sammarruca, Ph.D.; Leah Bergman, Ph.D.;

Hirotachi Abo, Ph.D.

Department Administrator: John Hiller, Ph.D.

May 2021

Authorization to Submit Dissertation

This dissertation of Hamdah Alanazi, submitted for the Degree of Doctor of Philosophy with a major in Physics and titled "The Relevance of Contact Terms Versus Pion-Exchange Contributions in the Chiral Effective Field Theory Description of Nucleon-Nucleon Scattering," has been reviewed in final form. Permission, as indicated by the signatures and dates given below, is now granted to submit final copies to the College of Graduate Studies for approval.

Major Professor: _____Date_____
Ruprecht Machleidt, Ph.D.

Committee Members: _____Date_____
Francesca Sammarruca, Ph.D.

_____Date_____
Leah Bergman, Ph.D.

_____Date_____
Hirotachi Abo, Ph.D.

Department Administrator: _____Date_____
John Hiller, Ph.D.

Abstract

The standard way to demonstrate the relevance of chiral symmetry for the NN interaction is to consider higher partial waves of NN scattering which are ruled entirely by chiral symmetry alone (since contacts vanish). However, in applications of NN-potentials to nuclear structure and reactions, the lower partial waves ($\mathrm{L} \leq 2$) are the important ones, generating the largest contributions. These lower partial waves are ruled by the dynamics at short range, and so, when the short-range contacts were to dominate over the chiral pion contributions in lower partial waves, then the predictions from "chiral potentials" would have little to do with chiral symmetry. In this thesis, we address this issue and investigate systematically the role of the (chiral) one- and two-pion exchanges, on the one hand, and the effect of the contacts, on the other hand, in the lower partial waves of NN scattering. Our study has also a pedagogical spin-off as it demonstrates in detail how the reproduction of the lower partial-wave phase shifts comes about from the various ingredients of the theory.

Acknowledgements

I would like to thank Dr. Machleidt for his support and invaluable guidance throughout my graduate studies. I am also thankful to my committee member, Dr. Sammarruca, for her help, support, and suggestions. Moreover, I thank my other committee members, Dr. Bergman and Dr. Abo. Finally, This work was supported in part by the U.S. Department of Energy under Grant No. DE-FG02-03ER41270.

Table of Contents

List of Tables

List of Figures

Chapter 1

Introduction

1.1 Historical perspective

The theory of nuclear forces has a long history. In 1911, Rutherford discovered the atomic nucleus by showing that a positively charged core with a small radius can describe the large angle alpha particle scattering [1]. Then, Thomson discovered the existence of isotopes while studying nuclear mass [2]. At this time, the first nuclear models assumed that the electrostatic forces between protons and electrons can be the reason to keep the nucleus together [2, 3]. In 1932, Chadwick discovered the neutron [4]. This implied that neutrons and protons are the basic components of the atomic nucleus. Consequently, the electromagnetic forces cannot be the reason why the nucleons bind together, because the repulsive electrical forces between protons would blow the nucleus apart. Therefore, a new force had to be considered to hold the nucleus together, which was called the nuclear force or the strong force [3].

Soon after, Wigner studied the binding energies of light nuclei and concluded that the nuclear force was strong within a short range [5]. Heisenberg [6] and Majorana [7] introduced the concept of "exchange forces" to explain how the nucleus can reach saturation. Around this period, experiment also made big progress, such as measuring the binding energy of the deuteron [8] and conducting proton-proton scattering experiments [9]. Heisenberg assumed that protons and neutrons are two different states of the same particle (nucleon), thus introducing what later was called the isospin formalism by Cassen and Condon in 1936 [10]. It was also suggested that the new force acts about equally strong between two protons, two neutrons, and proton and neutron, leading to the hypothesis of the charge independence of nuclear forces. Since then, various theories have been proposed to describe this force [3].

In 1935, Yukawa [11] created the first fundamental explanation for the nuclear force. Yukawa suggested that the nucleons (protons and neutrons) would exchange sub-nuclear

particles (eventually called mesons) between each other and this would create a force with a finite range. The potential equivalent to this force is proportional to $\exp(-mr)/r$.[1] The exponential contains the mass m of the exchanged particle (meson), and r is the distance between the centers of the two nucleons. However, the nuclear force turns out to be much more complicated because of its dependence on the spins of the two interacting nucleons. There have been many modifications of the meson-exchange theory of nuclear forces, but the basic concept developed by Yukawa proved to be right.

Yukawa's theory was extended and further modifications were made by Proca [12] and Kemmer [13]. They added pseudoscalar, pseudovector, and vector particles. In 1939, Rabi and co-workers discovered the quadrupole moment of the deuteron and, also, measured its magnetic moment [14]. Thus, it was realized that a tensor force was needed to describe the quadrupole moment of the deuteron. Such a tensor force can be created by either pseudoscalar or vector exchange. In 1946, Pauli [15] predicted that the meson was most likely an isovector pseudoscalar particle. A year later, the pion, with a mass of about 140 MeV, was found in cosmic rays by Occhialini and collaborators [16, 17]. It was also recognized, by Breit [18, 19] and Rosenfeld [20], that vector and scalar fields create a spin-orbit force, which was required to explain the structure of some light nuclei.

In 1951, Taketani, Nakamura, and Sasaki introduced their historic suggestion of dividing the nuclear force into three regions [21]. They distinguished between a short range ($r \leq 1$ fm), an intermediate range (1 fm $\leq r \leq 2$ fm), and a long range ($r \geq 2$ fm) region; where r denotes the distance between the centers of the two nucleons. In the long range, the one pion exchange (1PE) is dominant due to the small mass of the pion. The most important contribution in the intermediate range is the two-pion exchange (2PE), but also heavier mesons become relevant. Finally, in the short range, different processes play a role for the interaction; for example, there are multi-pion exchanges, heavy mesons, and potentially genuine quark-gluon exchanges [3].

[1] Throughout this thesis, we use units such that $\hbar = c = 1$.

In the 1950's, the 1PE became well established as the long range part of the nuclear force. The 1PE contribution to the nuclear force had all the features a physicist could want from a theory, namely, easy to calculate and successful in explaining data. Next, the two pion exchange (2PE) was considered which, however, created many problems. The efforts of pion theoretical potentials are divided into two groups: Taketani-Machida-Onuma evaluated an S-matrix directly from meson field theory [22], while the Brueckner-Watson method was based on an expansion in the particle number and derived a potential [23]. The main differences between the two groups came from the box diagrams and the pair terms. Pair terms denote contributions that include virtual nucleon-antinucleon states, also known as Z-graphs. However, the pair terms lead to a πN scattering length that is too large by about two orders of magnitude [3]. Therefore, the suppression of virtual pairs was assumed to be a general rule of meson theory [24]. We will pick up this aspect later on when we introduce the concept of chiral symmetry. In summary, the situation in the 1950's was that, while the 1PE turned out to be very useful in explaining nucleon-nucleon (NN) scattering data and the properties of the deuteron, multipion exchange could not be treated in a satisfactory way. Thus, the pion theories of the 1950's are generally judged to be failures.

The situation was "rescued" in the early 1960's by the discovery of heavy mesons, in particular the ρ [25] and ω [26]. The ρ is a 2π and the ω is a 3π resonance, with masses around $770 - 780$ MeV. As a consequence, the one-boson exchange (OBE) model was developed [27]. This model is based on the old Yukawa idea that the nuclear force is meson mediated. It turned out that the NN data can be described very well within the OBE model [3, 27–30].

In the 1970's, dispersion relations and field theoretical approaches were pursued to further develop the meson theory of nuclear forces. One of the most elaborate models applying dispersion relations was developed by the Paris group [31]. Dispersion theory deals with physically observable quantities only.

Lomon and Partovi [32] worked on a field theoretic model and evaluated the contributions from 2π-exchange Feynman diagrams to the NN interaction. Moreover, around the mid 1970s, a group of researchers at the University of Bonn, Germany, started a program directed towards the calculation of multipion exchange diagrams including nucleon resonances using field theory. Machleidt, Holinde, and Elster calculated two- and some three- and four-pion exchange diagrams and extended the model to take the effects of virtual isobar excitations into account [33]. The Bonn-potential accurately reproduces the NN scattering data and the properties of the deuteron. The Jülich group attempted to incorporate further correlated meson-exchange, for example, $\pi\pi$ and $\pi\rho$ [34, 35].

In the late 1980's and early 1990's, the Nijmegen group performed an excellent partial-wave analysis (PWA) of all *pp* and *np* scattering data below 350 MeV [36]. This triggered the development of the high-precision potentials of the 1990's [37–39] that fit the proton-proton (*pp*) and neutron-proton (*np*) scattering data below 350 MeV laboratory energy with a χ^2/datum close to one.

One of these high-precision NN potentials is the Charge-Dependent Bonn (CD-Bonn) potential [39], the off-shell behavior of which is based upon the *relativistic* OBE model. This creates non-locality which increases the triton binding energy. The Argonne group's high-precision potential (AV18) uses the local version of 1PE and local phenomenology for the intermediate and short range [38].

Because of the differences in the derivation of the various models for the nuclear force, there are differences off-shell. Due to those off-shell differences, the binding energy of the triton varies remarkably when calculations are executed with different two-nucleon forces (2NF) [3]. The missing binding energy is, generally, attributed to three-nucleon forces. Three-nucleon physics is reviewed in [40].

Despite the very successful description of most of the experimental data, the meson-exchange based NN potentials are essentially phenomenological models because mesons are not fundamental particles. A fundamental approach to the nuclear force has to start from quantum chromodynamics (QCD) [41], as to be discussed in Chapter 2.

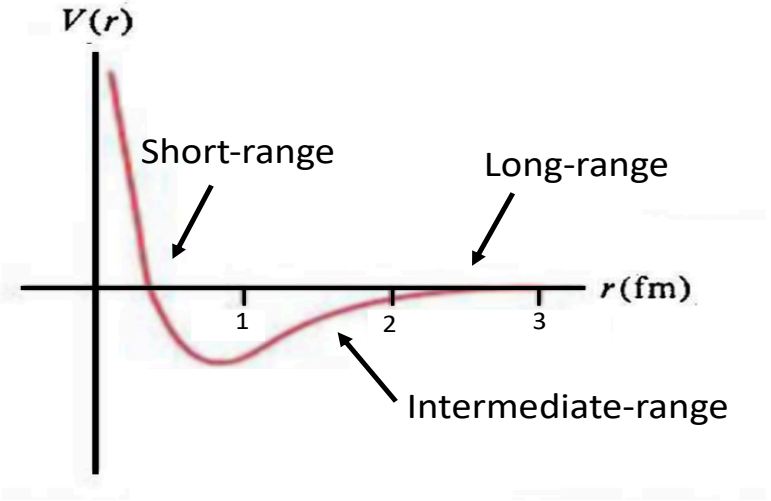

Figure 1.1: The nuclear potential and the three ranges of the nuclear force

.

1.2 Properties of the nuclear force

The nuclear force has many intriguing properties. As discussed, the nuclear potential depends on the range and can be divided into three parts [21] (cf. Fig 1.1). The long-range part is mediated by 1PE. In the intermediate range, 2PE dominates. Finally, at the short range, there are multi-pion exchanges, heavy mesons and, potentially, quark-gluon effects.

The nuclear force is spin dependent. The earliest evidence came from the non-vanishing quadrupole moment of the deuteron. This requires a tensor force which depends on the orientations of the spins of the two nucleons. Moreover, there is a strong spin-orbit force needed to explain the polarization data of NN scattering. The shell-model of the atomic nucleus provides further evidence for the nuclear spin-orbit force.

As we are dealing with the spin dependence of the nuclear force, we should also mention that there is a spin-spin force which, however, is not as important as the other forces components. Furthermore, the nuclear force is isospin dependent.

1.3 The purpose of this thesis

Since quantum chromodynamics (QCD) is the fundamental theory of strong interactions, the most fundamental approach to nuclear forces should be based upon QCD. Since direct QCD calculations are very involved and can only be conducted with brute computational power (lattice QCD [42, 43]), an effective field theory (EFT) has been developed that is based on the symmetries of low-energy QCD, particularly, chiral symmetry [41, 44–46]. These modern advances will be explained in more detail in Chapters 2 and 3. In the chiral EFT approach to nuclear forces, a clear distinction is made between the long- and short-range parts of the NN potential (where the long-range part includes the intermediate-range part). While the long-range part is given by one- and multi-pion exchanges (ruled by chiral symmetry), the short-range description consist of polynomials of increasing degree, also known as contact terms (since the short-range nucleon structure cannot be resolved at the low energy scale characteristic for traditional nuclear physics). Although chiral EFT based NN potentials have been around already for more than two decades, the exact role of the (short-ranged) contact terms *versus* the (long-ranged) pion-exchanges in the quantitative description of lower partial waves ($L \lesssim 2$) has never been clearly investigated. Note that in those lower partial waves, the contacts as well as pion-exchanges contribute, while in higher partial waves ($L \gtrsim 3$) only pion exchanges (and no contacts) are involved. Thus, it is easy to investigate the role of pion-exchanges in higher partial waves, and such analyses have been conducted repeatedly in the past [47–49]. However, the story is more complicated in lower partial waves, since the contributions from contacts and pion-exchanges need to be disentangled to obtain a clear idea of the role of both.

Such low partial wave analysis is important for the following reasons: Since lower partial waves are more sensitive to the short range potential, one may suspect that the contact contributions are dominant and simply override the pion-exchange contributions in lower partial waves. Note again that only the pion-contributions are ruled by chiral

symmetry, while the contacts are based on just the usual non-relativistic invariances and have nothing to do with chiral symmetry.

In applications of NN-potentials to nuclear structure and reactions, the lower partial waves make large contributions. Thus, if chiral symmetry would rule only the higher partial waves while the lower partial wave were essentially governed by the contacts, then the predictions from these "chiral" potentials for nuclear structure and reactions would have little to do with chiral symmetry.

Motivated by the above concerns, the purpose of this thesis is to systematically investigate the role of the contacts, on the one hand, and the effect of the (chiral) one- and two-pion exchange contributions, on the other hand, in the lower partial waves of chiral NN potentials; to determine if chiral symmetry plays an essential role in those lower waves.

In Chapter 2, we explain the foundation for chiral EFT and, in Chapter 3, we spell out in detail the chiral NN potential construction. Finally, in Chapter 4, the investigation of the central issue of this thesis is conducted. Chapter 5 concludes the thesis.

Chapter 2

Chiral effective field theory

2.1 An effective field theory for low energy QCD

Originally, meson theory was believed to be the fundamental theory of strong interactions with mesons being the field quanta in analogy to the photon in quantum electrodynamics (QED). In QED, electrically charged particles exchange photons to create the electromagnetic force. However, nowadays, quantum chromodynamics (QCD) is perceived to be the fundamental theory of strong interactions. QCD deals with color-charged quarks, which exchange gluons to create the strong force and, so, the degrees of freedom are quarks and gluons in QCD. QED and QCD are categorized as Abelian and non-Abelian gauge theories, respectively [41].

The force between quarks is weak at short distances corresponding to high energies. But the force is strong at long distances (low energies). Therefore, QCD allows for perturbative calculations at high energies, whereas in the low energy regime it is highly non-perturbative and therefore not solvable analytically in term of the fundamental degrees of freedom. For the nuclear force, the problem with QCD in the low energy regime was solved by Weinberg in 1979 [44]. He developed an EFT that is equivalent to low-energy QCD. This EFT uses pions and nucleons as the effective degrees of freedom instead of quarks and gluons. A theorem by Weinberg, which became known as "Folk Theorem," established a strong link between QCD and EFT that is given by observing all relevant symmetries of the underlying theory [44, 50–52].

In summary, the EFT program consists of the following steps:

1. Identify the soft and hard scales, and the degrees of freedom appropriate for (low-energy) nuclear physics.

2. Identify the relevant symmetries of low-energy QCD and investigate if and how they are broken.

3. Construct the most general Lagrangian consistent with those symmetries and sym-

metry breakings.

4. Design an organizational scheme that can distinguish between more and less important contributions: a low-momentum expansion.

5. Guided by the expansion, calculate Feynman diagrams for the problem under consideration to the desired accuracy.

The first step on the above list is to identify a separation of scales. In the hadron spectrum, a large gap between the masses of the pions (140 MeV) and the masses of the vector mesons, like $\rho(770)$ and $\omega(782)$, can clearly be identified. Thus, it is natural to assume that the pion mass sets the soft scale, $Q \sim m_\pi$, and the ρ mass the hard scale, $\Lambda_\chi \sim m_\rho$, also known as the chiral symmetry breaking scale. This is suggestive of considering an expansion in terms of the soft scale over the hard scale, Q/Λ_χ. Concerning the relevant degrees of freedom, it is reasonable to assume that nucleons and pions are the effective degrees of freedom for the ground state and the low energy spectrum of nuclei, instead of quarks and gluons.

The second step on the list requires the EFT to observe all relevant symmetries of low-energy QCD. In particular, chiral symmetry is of great importance here. This provides a link between QCD and chiral EFT and makes sure that this EFT is not just another phenomenology.

In the following subsections, we will discuss the further steps, one by one.

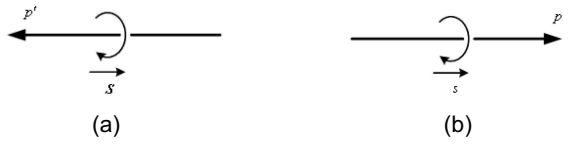

Figure 2.1: (a) Left handed chirality and (b) right handed chirality.

2.2 Chiral symmetry

Chirality and helicity

Chirality refers to the handedness of a particle with spin. There is also helicity, h, which is the projection of the spin of a particle onto (the unit-vector) of its momentum. A spin-1 particle can have $h = +1$ (right handed) if the direction of its spin is the same as the direction of its motion, or $h = -1$ (left handed) if the spin and motion are in opposite directions, cf. Fig. 2.1. Spin-$\frac{1}{2}$ particles have $h = \pm\frac{1}{2}$.

For particle with non-zero mass, the helicity can be altered by an observer. If we have an observer that moves at a velocity faster than the particle, the relative velocity will be directed in the opposite direction. In other words, one can convert a right-handed particle into a left-handed one simply by changing the frame of reference. However, helicity is conserved when the particle moves with the speed of light (massless particle), because there cannot be an observer traveling faster. The (conserved) Lorentz invariance helicity is called chirality.

The QCD Lagrangian

Nucleons are made from three up and down quarks. The interactions among quarks is described by QCD. This section will give an introduction to QCD, QCD symmetries and symmetry breakings. More details on this topic can be found in Refs. [41, 53]. The QCD

Lagrangian reads

$$\mathcal{L}_{QCD} = \bar{q}(i\gamma^\mu D_\mu - M)q - \frac{1}{4}\mathcal{G}_{\mu\nu,a}\mathcal{G}_a^{\mu\nu}\,, \tag{2.1}$$

where q denotes the quark fields. D_μ is the covariant derivative which is defined as

$$D_\mu = \partial_\mu - ig\frac{\lambda_a}{2}\,A_{\mu,a}\,, \tag{2.2}$$

where g denotes the strong coupling constant. The λ_a are the Gell-Mann matrices (3×3 matrices in color space), and $A_{\mu,a}$ are the gluon fields. The gluon field strength tensor is given by

$$\mathcal{G}_{\mu\nu,a} = \partial_\mu A_{\nu,a} - \partial_\nu A_{\mu,a} + g f_{abc} A_{\mu,b} A_{\nu,c}\,. \tag{2.3}$$

The f_{abc} are called the structure constants which form an antisymmetric tensor. The gluon-gluon term in the last equation is the reason for the peculiar features of the color force.

The masses of up, down, and strange quarks are small as compared to a typical hadronic scale:

$$\begin{aligned} m_u &= 2.2 \pm 0.6 \text{ MeV}, \\ m_d &= 4.7 \pm 0.5 \text{ MeV}, \\ m_s &= 96 \pm 8 \text{ MeV}. \end{aligned} \tag{2.4}$$

We now define the right and left handed quark fields:

$$q_R = P_R q\,, \qquad q_L = P_L q\,, \tag{2.5}$$

where P_R and P_L are projection operators defined as

$$P_R = \frac{1}{2}(1+\gamma_5)\,, \qquad P_L = \frac{1}{2}(1-\gamma_5)\,. \tag{2.6}$$

By using the left and right handed fields, we can write the QCD Lagrangian in the limit of vanishing quark masses as

$$\mathcal{L}^0_{QCD} = \bar{q}_R i\gamma^\mu D_\mu q_R + \bar{q}_L i\gamma^\mu D_\mu q_L - \frac{1}{4}\mathcal{G}_{\mu\nu,a}\mathcal{G}^{\mu\nu}_a \,. \tag{2.7}$$

Thus, the right and left handed components of massless quarks do not mix in the QCD Lagrangian. This is known as chiral symmetry for the two-flavor case. However, this symmetry is broken in two ways: explicitly and spontaneously.

2.2.1 Explicit symmetry breaking

The mass term $(-\bar{q}Mq)$ in the QCD Lagrangian breaks chiral symmetry explicitly. However, since the up and down quarks have very small masses as compared to the hadronic scale of ≈ 1 GeV, the breaking of chiral symmetry is small. So, we can say that QCD is approximately chirally symmetry. To better see this, we consider the quark mass matrix for the two-flavor case,

$$M = \begin{bmatrix} m_u & 0 \\ 0 & m_d \end{bmatrix} \tag{2.8}$$

$$= \frac{1}{2}(m_u + m_d)\begin{bmatrix} 1 & 0 \\ 0 & 1 \end{bmatrix} + \frac{1}{2}(m_u - m_d)\begin{bmatrix} 1 & 0 \\ 0 & -1 \end{bmatrix} \tag{2.9}$$

$$= \frac{1}{2}(m_u + m_d)I + \frac{1}{2}(m_u - m_d)\tau_3 \,. \tag{2.10}$$

The first term in the last equation is invariant under isospin symmetry and, so, isospin is an exact symmetry if $m_u = m_d$. Both terms break chiral symmetry explicitly. But, as discussed, because the quark masses are very small, the breaking is small [41, 50, 53].

2.2.2 Spontaneous symmetry breaking

Chiral symmetry is spontaneously broken because parity doublets do not exist in nature. For any hadron of positive parity, we would expect the same hadron with negative parity and vice versa. But these parity doublets are not observed in the low-energy hadron spectrum. For example, take the $\rho(770)$-meson which is a vector meson of negative parity and mass 775 MeV. There does exist a vector meson with positive parity, namely the $a_1(1260)$, but it has a mass of 1230 MeV and, therefore, does not represent a parity partner. A spontaneously broken symmetry generates a massless Goldstone boson. We identify the pions with those Goldstone bosons, which explains why the pion masses are so small. They are not exactly zero, because the up and down quark masses are not zero either. In summary, pions reflect spontaneous and explicit symmetry breaking.

2.3 Effective Lagrangians

The next step in the EFT program is to construct the most general Lagrangian consistent with those symmetries and symmetry breakings. An elegant formalism for the construction of such Lagrangians was developed by Callan *et al.* [54], who worked out the group-theoretical foundations of non-linear realizations of chiral symmetry. It is characteristic for these non-linear realizations that, whenever functions of the Goldstone bosons appear in the Lagrangian, they are always accompanied with at least one space-time derivative [44].

The relevant degrees of freedom are pions and nucleons. Since Goldstone bosons interact weakly at low energy and the interactions between them must vanish at zero momentum transfer and in the chiral limit ($m_\pi \to 0$), the low-energy expansion of the effective Lagrangian is arranged in powers of derivatives and pion masses. This effective Lagrangian is subdivided into the following pieces,

$$\mathcal{L}_{eff} = \mathcal{L}_{\pi\pi} + \mathcal{L}_{\pi N} + \mathcal{L}_{NN} + \cdots , \tag{2.11}$$

where $\mathcal{L}_{\pi\pi}$ deals with the dynamics among pions, $\mathcal{L}_{\pi N}$ describes the interaction between pions and a nucleon, and $\mathcal{L}_{NN}$ contains two-nucleon contact interactions which consist of four nucleon-fields (four nucleon legs) and no meson fields. The ellipsis stands for terms that involve two nucleons plus pions and three or more nucleons with or without pions, relevant for nuclear many-body forces. The individual Lagrangians are organized in terms of increasing orders [52]:

$$\mathcal{L}_{\pi\pi} = \mathcal{L}^{(2)}_{\pi\pi} + \mathcal{L}^{(4)}_{\pi\pi} + \cdots , \tag{2.12}$$

$$\mathcal{L}_{\pi N} = \mathcal{L}^{(1)}_{\pi N} + \mathcal{L}^{(2)}_{\pi N} + \mathcal{L}^{(3)}_{\pi N} + \mathcal{L}^{(4)}_{\pi N} + \cdots , \tag{2.13}$$

$$\mathcal{L}_{NN} = \mathcal{L}^{(0)}_{NN} + \mathcal{L}^{(2)}_{NN} + \mathcal{L}^{(4)}_{NN} + \cdots , \tag{2.14}$$

where the superscript refers to the number of derivatives or pion mass insertions (chiral dimension) and the ellipsis stands for terms of higher dimensions. These Lagrangians are, in part, very involved and have been published in the literature [41, 55]. Therefore, we will not reprint them here.

Chapter 3

The NN potential expansion

3.1 Chiral perturbation theory and power counting

Effective Langrangians lead to an infinite number of Feynman diagrams contributing to the interactions among nucleons. Therefore, we need a rule which distinguishes between large and small contributions. This scheme is called chiral perturbation theory (ChPT), which makes the theory manageable and calculable.

In ChPT, graphs are analyzed in terms of powers of small external momenta over the large scale: $(Q/\Lambda_\chi)^\nu$, where Q is generic for an external momentum (nucleon three-momentum or pion four-momentum) or a pion mass and $\Lambda_\chi \sim 1$ GeV is the chiral symmetry breaking scale (hardronic scale, hard scale). Determining the power ν has become known as power counting.

For the moment, we will consider only so-called irreducible graphs. By definition, an irreducible graph is a diagram that cannot be separated into two by cutting only nucleon lines. Following the Feynman rules of covariant perturbation theory, a nucleon propagator is Q^{-1}, a pion propagator Q^{-2}, each derivative in any interaction is Q, and each four-momentum integration Q^4. This is also known as naive dimensional analysis or Weinberg counting [45, 46].

Applying some topological identities, one obtains for the power of a connected irreducible diagram involving A nucleons

$$\nu = -2 + 2A - 2C + 2L + \sum_i \Delta_i, \tag{3.1}$$

with

$$\Delta_i \equiv d_i + \frac{n_i}{2} - 2, \tag{3.2}$$

where C denotes the number of separately connected pieces and L the number of loops in the diagram; d_i is the number of derivatives or pion-mass insertions and n_i the number of

nucleon fields (nucleon legs) involved in vertex i; the sum runs over all vertexes i contained in the diagram under consideration. Note that $\Delta_i \geq 0$ for all interactions allowed by chiral symmetry.

The most important observation from power counting is that the powers are bounded from below and, specifically, $\nu \geq 0$. This fact is crucial for the convergence of the low-momentum expansion.

Moreover, the power formula Eq. (3.1) allows to predict the leading orders of connected multi-nucleon forces. Consider a m-nucleon irreducibly connected diagram (m-nucleon force) in an A-nucleon system ($m \leq A$). The number of separately connected pieces is $C = A - m + 1$. Inserting this into Eq. (3.1) together with $L = 0$ and $\sum_i \Delta_i = 0$ yields $\nu = 2m - 4$. Thus, two-nucleon forces ($m = 2$) appear at $\nu = 0$. Three-nucleon forces ($m = 3$) at $\nu = 2$ (but they happen to cancel at that order), and four-nucleon forces at $\nu = 4$ (they don't cancel).

For an irreducible NN diagram ($A = 2, C = 1$), the power formula collapses to the very simple expression

$$\nu = 2L + \sum_i \Delta_i. \tag{3.3}$$

In summary, the chief point of the ChPT expansion is that, at a given order ν, there exists only a finite number of graphs. This is what makes the theory calculable. The expression $(Q/\Lambda_\chi)^{\nu+1}$ provides a rough estimate of the relative size of the contributions left out and, thus, of the precision at order ν. The ability to calculate observables to any degree of precision gives the theory its predictive power [41, 56].

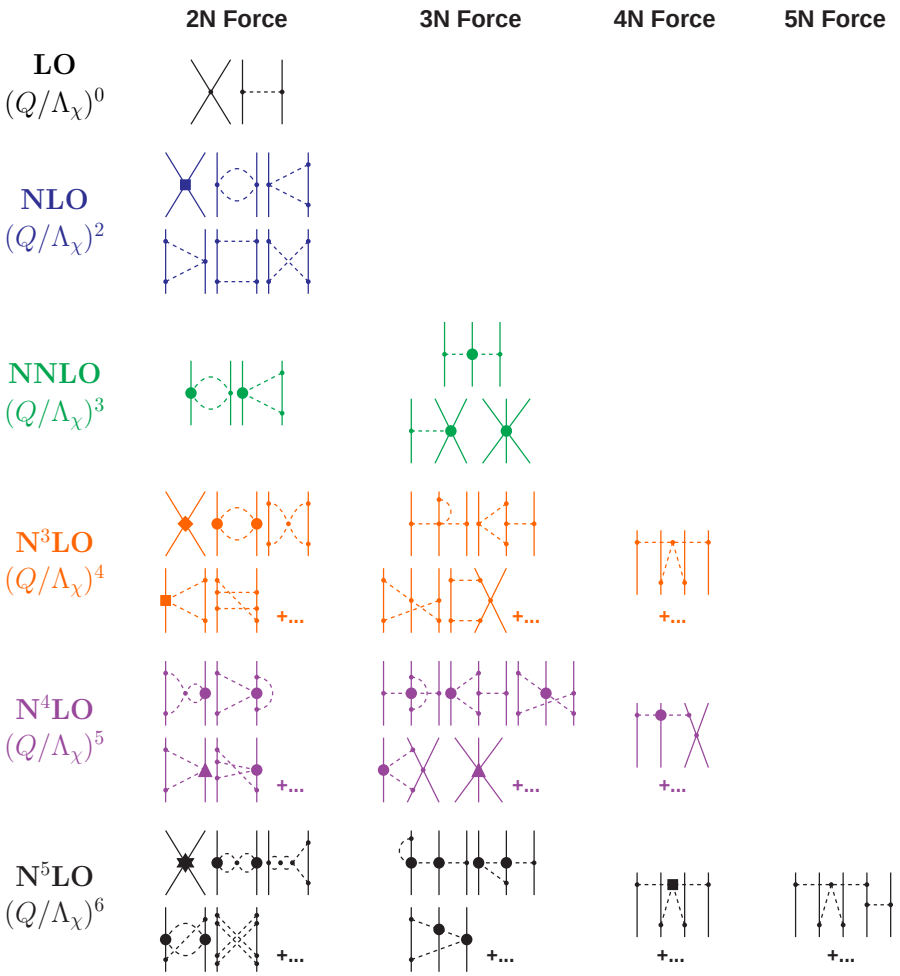

Figure 3.1: Hierarchy of nuclear forces in ChPT. Solid lines represent nucleons and dashed lines pions. Small dots, large solid dots, solid squares, triangles, diamonds, and stars denote vertices of index $\Delta_i = 0, 1, 2, 3, 4$ and 6, respectively.

3.2 The hierarchy of nuclear forces

Chiral perturbation theory and power counting imply that nuclear forces evolve as a hierarchy ruled by the power ν, see Fig. 3.1. We will focus here on the two-nucleon force (2NF). See Appendix A for details.

3.3 The long-range NN potential

Pion exchanges build up the long-range part of the NN potential. The various pion-exchange contributions can be arranged according to the number of pions being exchanged between the two nucleons:

$$V_\pi = V_{1\pi} + V_{2\pi} + V_{3\pi} + \cdots , \tag{3.4}$$

where the meaning of the subscripts is obvious and the ellipsis represents 4π and higher pion exchanges. For each of the above terms, we have a low-momentum expansion:

$$V_{1\pi} = V_{1\pi}^{(0)} + V_{1\pi}^{(2)} + V_{1\pi}^{(3)} + V_{1\pi}^{(4)} + V_{1\pi}^{(5)} + \cdots \tag{3.5}$$

$$V_{2\pi} = V_{2\pi}^{(2)} + V_{2\pi}^{(3)} + V_{2\pi}^{(4)} + V_{2\pi}^{(5)} + \cdots \tag{3.6}$$

$$V_{3\pi} = V_{3\pi}^{(4)} + V_{3\pi}^{(5)} + \cdots , \tag{3.7}$$

where the superscript denotes the order ν of the expansion. Due to parity and time reversal, there are no first order contributions.

Order by order, the long-range NN potential builds up as follows:

$$V_{L\Omega} \equiv V^{(0)} = V_{1\pi}^{(0)} \tag{3.8}$$

$$V_{NL\Omega} \equiv V^{(2)} = V_{L\Omega} + V_{1\pi}^{(2)} + V_{2\pi}^{(2)} \tag{3.9}$$

$$V_{NNL\Omega} \equiv V^{(3)} = V_{NL\Omega} + V_{1\pi}^{(3)} + V_{2\pi}^{(3)} \tag{3.10}$$

$$V_{N^3L\Omega} \equiv V^{(4)} = V_{NNL\Omega} + V_{1\pi}^{(4)} + V_{2\pi}^{(4)} + V_{3\pi}^{(4)} \tag{3.11}$$

$$V_{N^4L\Omega} \equiv V^{(5)} = V_{N^3L\Omega} + V_{1\pi}^{(5)} + V_{2\pi}^{(5)} + V_{3\pi}^{(5)} \tag{3.12}$$

where LΩ stands for leading order, NLΩ for next-to-leading order, etc..

Table 3.1: Basic constants used throughout this work [57].

Quantity	Value
Axial-vector coupling constant g_A	1.29
Pion-decay constant f_π	92.4 MeV
Charged-pion mass $m_{\pi^\pm}$	139.5702 MeV
Neutral-pion mass m_{π^0}	134.9766 MeV
Average pion-mass $\bar{m}_\pi$	138.0390 MeV
Proton mass M_p	938.2720 MeV
Neutron mass M_n	939.5654 MeV
Average nucleon-mass $\bar{M}_N$	938.9183 MeV

3.3.1 One-pion exchange (1PE)

At leading order (LΩ), only one-pion exchange (1PE) contributes to the long range, cf. Figs. 3.1 and 3.2. The charge-independent 1PE is given by

$$V_{1\pi}^{(CI)}(\vec{p'},\vec{p}) = -\frac{g_A^2}{4f_\pi^2}\,\boldsymbol{\tau}_1\cdot\boldsymbol{\tau}_2\,\frac{\vec{\sigma}_1\cdot\vec{q}\;\vec{\sigma}_2\cdot\vec{q}}{q^2+m_\pi^2}\,. \tag{3.13}$$

where $\vec{p'}$ and $\vec{p}$ denote the final and initial nucleon momenta in the center-of-mass system (CMS), respectively. $\vec{\sigma}_{1,2}$ and $\boldsymbol{\tau}_{1,2}$ are the spin and isospin operators of nucleons 1 and 2. Parameters g_A, f_π and m_π denote the axial-vector coupling constant, pion-decay constant, and the pion mass, respectively. See Table 3.1 for their values. Higher order corrections to the 1PE are taken care of by mass and coupling constant renormalizations $g_A/f_\pi \to g_{\pi N}/M_N$. Note also that, on shell, there are no relativistic corrections. Thus, we apply 1PE in the form of Eq. (3.13) through all orders.

The 1PE potential, Eq. (3.13), can be re-written as follows:

$$V_{1\pi}^{(CI)}(\vec{p'},\vec{p}) = -\frac{g_A^2}{12f_\pi^2}\,\boldsymbol{\tau}_1\cdot\boldsymbol{\tau}_2\left(\vec{\sigma}_1\cdot\vec{\sigma}_2\;-\;\vec{\sigma}_1\cdot\vec{\sigma}_2\,\frac{m_\pi^2}{q^2+m_\pi^2}+\;\frac{S_{12}(\vec{q})}{q^2+m_\pi^2}\;\right), \tag{3.14}$$

with tensor operator

$$S_{12}(\vec{q}) = 3\,\vec{\sigma}_1\cdot\vec{q}\;\vec{\sigma}_2\cdot\vec{q}\;-\;\vec{\sigma}_1\cdot\vec{\sigma}_2\,q^2\,, \tag{3.15}$$

where the 1PE is broken up into a spin-spin contact term (δ-function term), a spin-spin Yukawa central force, and a tensor piece. The 1PE tensor force is known to be strong, while the spin-spin central force is weak.

If one takes the charge-dependence of the 1PE into account, then, in proton-proton (pp) and neutron-neutron (nn) scattering, one has

$$V_{1\pi}^{(pp)}(\vec{p'},\vec{p}) = V_{1\pi}^{(nn)}(\vec{p'},\vec{p}) = V_{1\pi}(m_{\pi^0}) \tag{3.16}$$

and, in neutron-proton (np) scattering,

$$V_{1\pi}^{(np)}(\vec{p'},\vec{p}) = -V_{1\pi}(m_{\pi^0}) + (-1)^{I+1}\, 2\, V_{1\pi}(m_{\pi^\pm})\,, \tag{3.17}$$

where $I = 0, 1$ denotes the total isospin of the two-nucleon system and

$$V_{1\pi}(m_\pi) = -\,\frac{g_A^2}{4f_\pi^2}\,\frac{\vec{\sigma}_1\,\cdot\,\vec{q}\,\vec{\sigma}_2\,\cdot\,\vec{q}}{q^2+m_\pi^2}\,, \tag{3.18}$$

with $m_{\pi^0} = 134.9766$ MeV and $m_{\pi^\pm} = 139.5702$ MeV.

The charge-dependence of the 1PE is of order (NLΩ), but we include it already at leading order (LΩ) to make the comparison with the np phase-shift analyses meaningful.

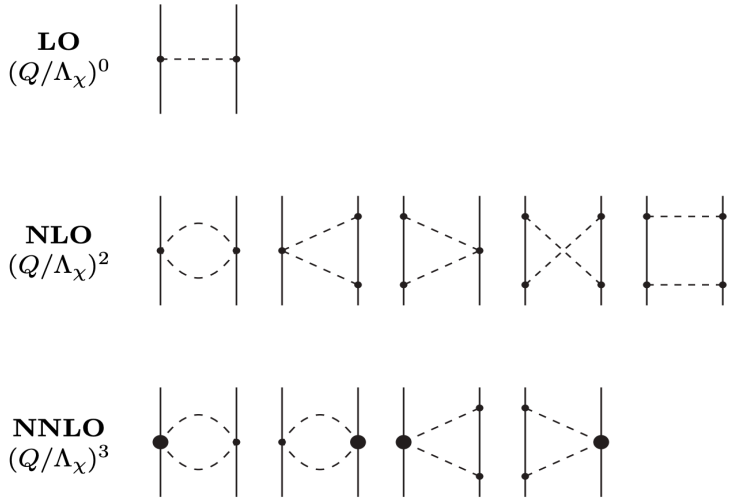

Figure 3.2: LΩ, NLΩ, and NNLΩ contributions to the NN interaction. Notation as in Fig. 3.1.

3.3.2 Two-pion exchange (2PE)

To state the mathematical expressions for the 2PE contributions, we use the following general scheme:

$$\begin{aligned} V_{2\pi}^{(\nu)}(\vec{p'},\vec{p}) = \; & V_C^{(\nu)} + \boldsymbol{\tau}_1 \cdot \boldsymbol{\tau}_2 \, W_C^{(\nu)} \\ & + [\, V_S^{(\nu)} + \boldsymbol{\tau}_1 \cdot \boldsymbol{\tau}_2 \, W_S^{(\nu)} \,] \, \vec{\sigma}_1 \cdot \vec{\sigma}_2 \\ & + [\, V_{LS}^{(\nu)} + \boldsymbol{\tau}_1 \cdot \boldsymbol{\tau}_2 \, W_{LS}^{(\nu)} \,] \, (-i\vec{S} \cdot (\vec{q} \times \vec{k})) \\ & + [\, V_T^{(\nu)} + \boldsymbol{\tau}_1 \cdot \boldsymbol{\tau}_2 \, W_T^{(\nu)} \,] \, \vec{\sigma}_1 \cdot \vec{q} \, \vec{\sigma}_2 \cdot \vec{q} \\ & + [\, V_{\sigma L}^{(\nu)} + \boldsymbol{\tau}_1 \cdot \boldsymbol{\tau}_2 \, W_{\sigma L}^{(\nu)} \,] \, \vec{\sigma}_1 \cdot (\vec{q} \times \vec{k}) \, \vec{\sigma}_2 \cdot (\vec{q} \times \vec{k}) \,, \end{aligned} \tag{3.19}$$

where $\vec{p'}$ and $\vec{p}$ denote the final and initial nucleon momenta in the CMS; moreover,

$\vec{q} \equiv \vec{p'} - \vec{p}$ is the momentum transfer,

$\vec{k} \equiv \frac{1}{2}(\vec{p'} + \vec{p})$ the average momentum, and

$\vec{S} \equiv \frac{1}{2}(\vec{\sigma}_1 + \vec{\sigma}_2)$ the total spin.

For on-shell scattering, V_α and W_α ($\alpha = C, S, LS, T, \sigma L$) can be expressed as functions of $q = \mid \vec{q} \mid$ and $p = \mid \vec{p'} \mid = \mid \vec{p} \mid$, only.

Next-to-leading order (NLΩ)

Using the above scheme, the NN diagrams that occur at NLΩ (cf. Figs. 3.1 and 3.2) contribute in the following way [47, 48]:

$$W_C^{(2)} = \frac{L(\tilde{\Lambda};q)}{384\,\pi^2\,f_\pi^4}\left[4m_\pi^2(1+4g_A^2-5g_A^4)+q^2(1+10g_A^2-23g_A^4)-\frac{48g_A^4m_\pi^4}{w^2}\right] + \text{polynomial terms of order two}\,, \tag{3.20}$$

$$V_T^{(2)} = -\frac{1}{q^2}V_S = -\frac{3g_A^4}{64\pi^2 f_\pi^4}L(\tilde{\Lambda};q) + \text{polynomial terms of order zero}\,, \tag{3.21}$$

where the regularized logarithmic loop function is given by

$$L(\tilde{\Lambda};q) = \frac{w}{2q}\,\ln\frac{\tilde{\Lambda}^2(2m_\pi^2+q^2)\,-2m_\pi^2q^2\,+\tilde{\Lambda}\sqrt{\tilde{\Lambda}^2-4m_\pi^2}\,q\,w}{2m_\pi^2(\tilde{\Lambda}^2+q^2)} \tag{3.22}$$

with

$$w \equiv \sqrt{4m_\pi^2+q^2}\,. \tag{3.23}$$

For the explicit expressions of the polynomial terms that contribute in Eqs. (3.20) and (3.21), see Ref. [47].

Next-to-next-to-leading order (NNLΩ)

The NNLΩ contribution, included in Fig. 3.2, is given by [47, 48]:

$$V_C^{(3)} = \frac{3g_A^2}{16\,\pi\,f_\pi^4}[2m_\pi^2(c_3-2c_1)+c_3q^2]\,(2m_\pi^2+q^2)A(\tilde{\Lambda};q) + \text{polynomial terms of order three}\,, \tag{3.24}$$

$$W_T^{(3)} = -\frac{1}{q^2}W_S = -\frac{g_A^4}{32\,\pi\,f_\pi^4}c_4w^2\,A(\tilde{\Lambda};q)\,+\text{polynomial terms of order one}\,. \tag{3.25}$$

The loop function that appears in the above expressions, regularized by spectral-function cut-off $\tilde{\Lambda}$, is

$$A(\tilde{\Lambda};q) = \frac{1}{2q}\,\arctan\,\frac{q(\tilde{\Lambda}-2m_\pi)}{q^2+2\tilde{\Lambda}m_\pi}\,. \tag{3.26}$$

For the explicit expressions of the polynomial terms that contribute in Eqs. (3.24) and (3.25), see Ref. [47].

Next-to-next-to-next-to-leading order ($\mathbf{N^3L\Omega}$)

Football diagram at $\mathbf{N^3L\Omega}$ The football diagram at $\mathrm{N^3L\Omega}$, Fig. 3.3(a), generates [48, 58]

$$V_C^{(4)} = \frac{3}{16\pi^2 f_\pi^4}\left\{\left[\frac{c_2}{6}w^2 + c_3(2m_\pi^2+q^2) - 4c_1 m_\pi^2\right]^2 + \frac{c_2^2}{45}w^4\right\}L(\tilde{\Lambda};q), \tag{3.27}$$

$$W_T^{(4)} = -\frac{1}{q^2}\,W_S = \frac{c_4^2}{96\pi^2 f_\pi^4}w^2\,L(\tilde{\Lambda};q). \tag{3.28}$$

We note that in addition to the non-polynominal terms shown in the above equations, there are polynomial terms of order four in the central potential and polynomial terms of order two in the tensor and spin-orbit potentials, which we do not show explicitly. This note applies to all potential expressions of order $\mathrm{N^3L\Omega}$.

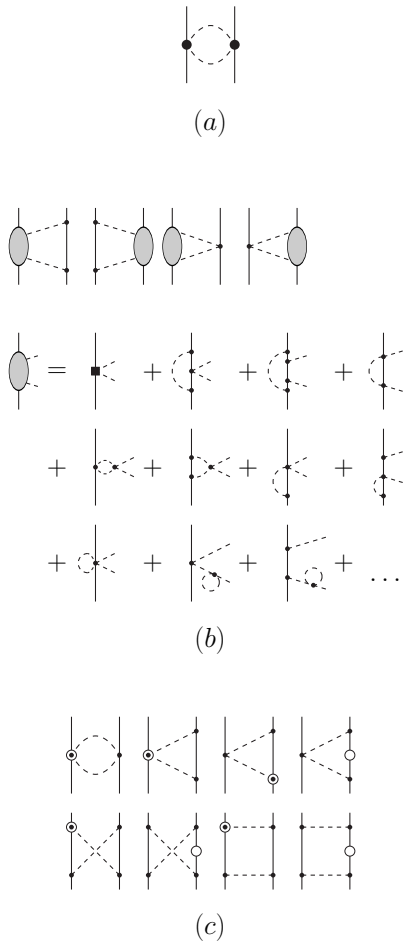

Figure 3.3: Two-pion-exchange contributions at $\mathrm{N^3L}\Omega$ with (a) the $\mathrm{N^3L}\Omega$ football diagram, (b) the leading 2PE two-loop contributions, and (c) the relativistic corrections of $\mathrm{NL}\Omega$ diagrams. Notation as in Fig. 3.1. Open circles denote relativistic $1/M_N$ corrections.

Leading two-loop contributions The leading-order 2π-exchange two-loop diagrams are shown in Fig. 3.3(b). In terms of spectral functions, the results are [48, 58]:

$$\begin{aligned}
\mathrm{Im}\, V_C^{(4)} =& \frac{3g_A^4(2m_\pi^2 - \mu^2)}{\pi\mu(4f_\pi)^6}\left[(m_\pi^2 - 2\mu^2)\left(2m_\pi + \frac{2m_\pi^2 - \mu^2}{2\mu}\ln\frac{\mu + 2m_\pi}{\mu - 2m_\pi}\right)\right. \\
&\left. + 4g_A^2 m_\pi\,(2m_\pi^2 - \mu^2)\right], \qquad (3.29)\\
\mathrm{Im}\, W_C^{(4)} =& \frac{2k}{3\mu(8\pi f_\pi^2)^3}\int_0^1 dx[g_A^2(\mu^2 - 2m_\pi^2) \\
&+ 2(1 - g_A^2)k^2x^2]\Big\{96\pi^2 f_\pi^2\,[2m_\pi^2 - \mu^2)(\bar{d}_1 + \bar{d}_2 - 2k^2x^2\bar{d}_3 + 4m_\pi^2\bar{d}_5] \\
&+ [4m_\pi^2(1 + 2g_A^2) - \mu^2(1 + 5g_A^2)]\frac{k}{\mu}\ln\frac{\mu + 2k}{2m_\pi} + \frac{\mu^2}{12}(5 + 13g_A^2) - 2m_\pi^2(1 + 2g_A^2) \\
&- 3k^2x^2 + 6kx\sqrt{m_\pi^2 + k^2x^2}\ln\frac{kx + \sqrt{m_\pi^2 + k^2x^2}}{m_\pi} \\
&+ g_A^4(\mu^2 - 2k^2x^2 - 2m_\pi^2)\left[\frac{5}{6} + \frac{m_\pi^2}{k^2x^2} - \left(1 + \frac{m_\pi^2}{k^2x^2}\right)^{3/2}\ln\frac{kx + \sqrt{m_\pi^2 + k^2x^2}}{m_\pi}\right]\Big\}, \qquad (3.30)
\end{aligned}$$

$$\begin{aligned}
\mathrm{Im}\, V_S^{(4)} =& \mu^2\,\mathrm{Im}\, V_T = \frac{g_A^2\mu k^3}{8\pi f_\pi^4}(\bar{d}_{15} - \bar{d}_{14}) + \frac{2g_A^6\mu k^3}{(8\pi f_\pi^2)^3}\times \\
&\int_0^1 dx(1 - x^2)\left[\frac{1}{6} - \frac{m_\pi^2}{k^2x^2} + \left(1 + \frac{m_\pi^2}{k^2x^2}\right)^{3/2}\ln\frac{kx + \sqrt{m_\pi^2 + k^2x^2}}{m_\pi}\right], \qquad (3.31)\\
\mathrm{Im}\, W_S^{(4)} =& \mu^2\,\mathrm{Im}\, W_T(i\mu) = \frac{g_A^4(4m_\pi^2 - \mu^2)}{\pi(4f_\pi)^6}\left[\left(m_\pi^2 - \frac{\mu^2}{4}\right)\ln\frac{\mu + 2m_\pi}{\mu - 2m_\pi} + (1 + 2g_A^2)\mu m_\pi\right], \qquad (3.32)
\end{aligned}$$

where $k = (\mu^2/4 - m_\pi^2)^{1/2}$.

The momentum-space potentials $V_\alpha(q)$ and $W_\alpha(q)$ are obtained from the above expression by means of the subtracted dispersion integrals as follows [48]:

$$\begin{aligned}
V_{C.S}(q) =& -\frac{2q^6}{\pi}\int_{2m_\pi}^{\tilde{\Lambda}} d\mu\,\frac{\mathrm{Im}\, V_{C.S}(i\mu)}{\mu^5(\mu^2 + q^2)}, \\
V_T(q) =& \frac{2q^4}{\pi}\int_{2m_\pi}^{\tilde{\Lambda}} d\mu\,\frac{\mathrm{Im}\, V_T(i\mu)}{\mu^3(\mu^2 + q^2)}. \qquad (3.33)
\end{aligned}$$

We note that the subtracted dispersion integrals generate (besides the non-polynomial

contributions) also polynomial terms of order four for the central potential and polynomial terms of order two for the tensor potentials.

Leading relativistic corrections The relativistic corrections of the NLΩ diagrams, which are shown in Fig. 3.3(c), count as N^{3}LΩ and are given by [48]

$$V_C^{(4)} = \frac{3g_A^4}{128\pi f_\pi^4 M_N}\left[\frac{m_\pi^5}{2w^2} + (2m_\pi^2+q^2)(q^2-m_\pi^2)\,A(\tilde{\Lambda};q)\right], \tag{3.34}$$

$$W_C^{(4)} = \frac{g_A^2}{64\pi f_\pi^4 M_N}\left\{\frac{3g_A^2 m_\pi^5}{2w^2} + [g_A^2(3m_\pi^2+2q^2) - 2m_\pi^2 - q^2](2m_\pi^2+q^2)\,A(\tilde{\Lambda};q)\right\} \tag{3.35}$$

$$V_T^{(4)} = -\frac{1}{q^2}V_S = \frac{3g_A^4}{256\pi f_\pi^4 M_N}(5m_\pi^2+2q^2)\,A(\tilde{\Lambda};q), \tag{3.36}$$

$$W_T^{(4)} = -\frac{1}{q^2}W_S = \frac{g_A^2}{128\pi f_\pi^4 M_N}[g_A^2(3m_\pi^2+q^2) - w^2]\,A(\tilde{\Lambda};q), \tag{3.37}$$

$$V_{LS}^{(4)} = \frac{3g_A^4}{32\pi f_\pi^4 M_N}(2m_\pi^2+q^2)\,A(\tilde{\Lambda};q), \tag{3.38}$$

$$W_{LS}^{(4)} = \frac{g_A^2(1-g_A^2)}{32\pi f_\pi^4 M_N}w^2\,A(\tilde{\Lambda};q). \tag{3.39}$$

Subleading relativistic corrections We also add to $V_{N^3L\Omega}$ the $1/M_N$ corrections of the NNLΩ 2PE diagrams proportional to c_i, to compensate for the excessive attraction generated by the football diagram at N^{3}LΩ. This contribution is repulsive and proportional to c_i/M_N, Fig. 3.4. It appears nominally at fifth order and is given by [48, 58]:

$$\begin{aligned} V_C^{(4)} = \frac{g_A^2 L(\tilde{\Lambda};q)}{32\pi^2 M_N f_\pi^4}[&(6c_3-c_2)q^4 + 4(3c_3-c_2-6c_1)q^2m_\pi^2 \\ &+ 6(2c_3-c_2)m_\pi^4 - 24(2c_1+c_3)m_\pi^6 w^{-2}], \end{aligned} \tag{3.40}$$

$$W_C^{(4)} = -\frac{c_4}{192\pi^2 M_N f_\pi^4}[g_A^2(8m_\pi^2+5q^2)+w^2]q^2 L(\tilde{\Lambda};q), \tag{3.41}$$

$$W_T^{(4)} = -\frac{1}{q^2}W_S = \frac{c_4}{192\pi^2 M_N f_\pi^4}[w^2 - g_A^2(16m_\pi^2+7q^2)]L(\tilde{\Lambda};q), \tag{3.42}$$

$$V_{LS}^{(4)} = \frac{c_2 g_A^2}{8\pi^2 M_N f_\pi^4}w^2 L(\tilde{\Lambda};q), \tag{3.43}$$

$$W_{LS}^{(4)} = -\frac{c_4}{48\pi^2 M_N f_\pi^4}[g_A^2(8m_\pi^2+5q^2)+w^2]L(\tilde{\Lambda};q). \tag{3.44}$$

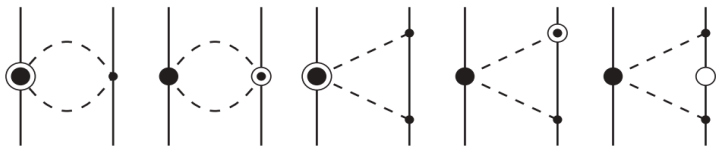

Figure 3.4: Relativistic corrections of NNLΩ diagrams.
Notation as in Fig. 3.3.

3.3.3 Three-Pion Exchange (3PE)

The 3PE contributions that occur at N^3LO have been calculated by the Munich group and found to be negligible [59, 60]. We therefore leave them out.

3.4 The short-range NN potential (NN contact terms)

In the EFT approach, the short-range interaction is described by contributions of the contact type, which are constrained by parity, time-reversal, and the usual invariances, but not by chiral symmetry. Only even powers of momentum are allowed because of parity and time-reversal. Thus, the expansion of the contact potential is formally given by

$$V_{ct} = V_{ct}^{(0)} + V_{ct}^{(2)} + V_{ct}^{(4)} + V_{ct}^{(6)} + \cdots \,, \tag{3.45}$$

where the superscript denotes the power or order.

In operator form, the contact potentials are given by:
Zeroth-order (leading order, LΩ),

$$V_{ct}^{(0)}(\vec{p'},\vec{p}) = C_S + C_T\, \vec{\sigma}_1 \cdot \vec{\sigma}_2 \,. \tag{3.46}$$

Second order (next-to-leading order, NLΩ),

$$\begin{aligned} V_{ct}^{(2)}(\vec{p'},\vec{p}) = {} & C_1 q^2 + C_2 k^2 + (C_3 q^2 + C_4 k^2)\vec{\sigma_1} \cdot \vec{\sigma_2} \\ & + C_5[-i\vec{S} \cdot (\vec{q} \times \vec{k})] + C_6(\vec{\sigma_1} \cdot \vec{q})(\vec{\sigma_2} \cdot \vec{q}) \\ & + C_7(\vec{\sigma_1} \cdot \vec{k})(\vec{\sigma_2} \cdot \vec{k}) \,. \end{aligned} \tag{3.47}$$

Fourth order (next-to-next-to-next-to-leading order, $\mathrm{N^3L\Omega}$):

$$\begin{aligned} V_{ct}^{(4)}(\vec{p}\,',\vec{p}) &= D_1 q^4 + D_2 k^4 + D_3 q^2 k^2 + D_4 (\vec{q}\times\vec{k})^2 \\ &+ [D_5 q^4 + D_6 k^4 + D_7 q^2 k^2 + D_8 (\vec{q}\times\vec{k})^2]\vec{\sigma_1}\cdot\vec{\sigma_2} \\ &+ (D_9 q^2 + D_{10} k^2)[-i\vec{S}\cdot(\vec{q}\times\vec{k}] \\ &+ (D_{11} q^2 + D_{12} k^2)(\vec{\sigma_1}\cdot\vec{q})(\vec{\sigma_2}\cdot\vec{q}) \\ &+ (D_{13} q^2 + D_{14} k^2)(\vec{\sigma_1}\cdot\vec{k})(\vec{\sigma_2}\cdot\vec{k}) \\ &+ D_{15}[\vec{\sigma_1}\cdot(\vec{q}\times\vec{k})\vec{\sigma_2}\cdot(\vec{q}\times\vec{k})]\,. \end{aligned} \tag{3.48}$$

In terms of a partial-wave decomposition, we have up to fourth order:

$$\begin{aligned} \langle {}^1S_0, p'|V_{ct}|{}^1S_0, p\rangle &= \widetilde{C}_{{}^1S_0} + C_{{}^1S_0}(p^2+p'^2) + \widehat{D}_{{}^1S_0}(p'^4+p^4) + D_{{}^1S_0} p'^2 p^2, \\ \langle {}^3S_1, p'|V_{ct}|{}^3S_1, p\rangle &= \widetilde{C}_{{}^3S_1} + C_{{}^3S_1}(p^2+p'^2) + \widehat{D}_{{}^3S_1}(p'^4+p^4) + D_{{}^3S_1} p'^2 p^2, \\ \langle {}^3S_1, p'|V_{ct}|{}^3D_1, p\rangle &= C_{{}^3S_1-{}^3D_1} p^2 + \widehat{D}_{{}^3S_1-{}^3D_1} p^4 + D_{{}^3S_1-{}^3D_1} p'^2 p^2, \\ \langle {}^1P_1, p'|V_{ct}|{}^1P_1, p\rangle &= C_{{}^1P_1}\, pp' + D_{{}^1P_1}(p'^3 p + p' p^3), \\ \langle {}^3P_0, p'|V_{ct}|{}^3P_0, p\rangle &= C_{{}^3P_0}\, pp' + D_{{}^3P_0}(p'^3 p + p' p^3), \\ \langle {}^3P_1, p'|V_{ct}|{}^3P_1, p\rangle &= C_{{}^3P_1}\, pp' + D_{{}^3P_1}(p'^3 p + p' p^3), \\ \langle {}^3P_2, p'|V_{ct}|{}^3P_2, p\rangle &= C_{{}^3P_2}\, pp' + D_{{}^3P_2}(p'^3 p + p' p^3), \\ \langle {}^3P_2, p'|V_{ct}|{}^3F_2, p\rangle &= D_{{}^3P_2-{}^3F_2} p' p^3, \\ \langle {}^1D_2, p'|V_{ct}|{}^1D_2, p\rangle &= D_{{}^1D_2} p'^2 p^2, \\ \langle {}^3D_1, p'|V_{ct}|{}^3D_1, p\rangle &= D_{{}^3D_1} p'^2 p^2, \\ \langle {}^3D_2, p'|V_{ct}|{}^3D_2, p\rangle &= D_{{}^3D_2} p'^2 p^2, \\ \langle {}^3D_3, p'|V_{ct}|{}^3D_3, p\rangle &= D_{{}^3D_3} p'^2 p^2. \end{aligned} \tag{3.49}$$

Notice that, in our notation, partial-wave contact LECs

- $\widetilde{C}_\alpha$ are of zeroth order (there are two),

- C_α are of second order (there are seven), and
- $\widehat{D}_\alpha$ and D_α are of fourth order (there are 15),

where α stands for a partial wave or a combination thereof. There exist linear one-to-one relations between the two $\widetilde{C}_\alpha$ and C_S and C_T of Eq. (3.46), the seven C_α and the seven C_i of Eq. (3.47), and the 15 $\widehat{D}_\alpha$ and D_α and the 15 D_i of Eq. (3.48). The relations can be found in Appendix B [41].

Note that the partial-wave decomposition of Q^ν (where Q is either the momentum transfer q or the average momentum k) has an interesting property. For even ν,

$$Q^\nu = f_{\frac{\nu}{2}}(\cos\theta)\,, \tag{3.50}$$

where f_m stands for a polynomial of degree m and θ is the center-of-mass scattering angle. The partial-wave decomposition of Q^ν for a state of orbital-angular momentum L involves the integral

$$I_L^{(\nu)} = \int_{-1}^{+1} Q^\nu P_L(\cos\theta) d\cos\theta = \int_{-1}^{+1} f_{\frac{\nu}{2}}(\cos\theta) P_L(\cos\theta) d\cos\theta\,, \tag{3.51}$$

where P_L is a Legendre polynomial. Due to the orthogonality of the P_L,

$$I_L^{(\nu)} = 0 \quad \text{for} \quad L > \frac{\nu}{2}\,. \tag{3.52}$$

Consequently, contact terms of order zero contribute only in S-waves, while second order terms can contribute up to P-waves, fourth order terms up to D-waves, etc..

3.5 Scattering equation and regularization

The full NN potential, calculated to a certain order, is given by the sum of long-range and short-range potentials as following [41, 56].,

$$V_{L\Omega} \equiv V^{(0)} = V_{1\pi} + V_{ct}^{(0)}, \tag{3.53}$$

$$V_{NL\Omega} \equiv V^{(2)} = V_{L\Omega} + V_{2\pi}^{(2)} + V_{ct}^{(2)}, \tag{3.54}$$

$$V_{NNL\Omega} \equiv V^{(3)} = V_{NL\Omega} + V_{2\pi}^{(3)}, \tag{3.55}$$

$$V_{N^3L\Omega} \equiv V^{(4)} = V_{NNL\Omega} + V_{2\pi}^{(4)} + V_{3\pi}^{(4)} + V_{ct}^{(4)}, \tag{3.56}$$

$$V_{N^4L\Omega} \equiv V^{(5)} = V_{N^3L\Omega} + V_{2\pi}^{(5)} + V_{3\pi}^{(5)}. \tag{3.57}$$

The potential V is, in principal, an invariant amplitude (with relativity taken into account perturbatively) and, thus, satisfies a relativistic scattering equation, like, e. g., the Blankenbeclar-Sugar (BbS) equation [61], which reads explicitly,

$$T(\vec{p}\,',\vec{p}) = V(\vec{p}\,',\vec{p}) + \int \frac{d^3p''}{(2\pi)^3}\, V(\vec{p}\,',\vec{p}\,'')\, \frac{M_N^2}{E_{p''}}\, \frac{1}{p^2 - p''^2 + i\epsilon}\, T(\vec{p}\,'',\vec{p}) \tag{3.58}$$

with $E_{p''} \equiv \sqrt{M_N^2 + p''^2}$ and M_N the nucleon mass. The advantage of using a relativistic scattering equation is that it automatically includes relativistic kinematical corrections to all orders. Thus, in the scattering equation, no propagator modifications are necessary when moving up to higher orders.

Defining

$$\widehat{V}(\vec{p'},\vec{p}) \equiv \frac{1}{(2\pi)^3}\sqrt{\frac{M_N}{E_{p'}}}\, V(\vec{p'},\vec{p})\sqrt{\frac{M_N}{E_p}} \tag{3.59}$$

and

$$\widehat{T}(\vec{p'},\vec{p}) \equiv \frac{1}{(2\pi)^3}\sqrt{\frac{M_N}{E_{p'}}}\, T(\vec{p'},\vec{p})\sqrt{\frac{M_N}{E_p}}, \tag{3.60}$$

the BbS equation collapses into the usual, nonrelativistic Lippmann-Schwinger (LS) equation,

$$\widehat{T}(\vec{p'},\vec{p}) = \widehat{V}(\vec{p'},\vec{p}) + \int d^3\, p''\, \widehat{V}(\vec{p'},\vec{p''})\, \frac{M_N}{p^2 - p''^2 + i\epsilon}\, \widehat{T}(\vec{p''},\vec{p})\,. \tag{3.61}$$

Iteration of $\widehat{V}$ in the LS equation, Eq. (3.61), requires cutting $\widehat{V}$ off for high momenta to avoid infinities. This is consistent with the fact that ChPT is a low-momentum expansion which is valid only for momenta $Q \leq \Lambda_\chi \approx 1$ GeV. Therefore, the potential $\widehat{V}$ is multiplied with a regulator function $f(p',p)$,

$$\widehat{V}(\vec{p'},\vec{p}) \longmapsto \widehat{V}(\vec{p'},\vec{p})\, f(p',p)\,, \tag{3.62}$$

with

$$f(p',p) = exp[-(p'/\Lambda)^{2n} - (p/\Lambda)^{2n}]. \tag{3.63}$$

For the chiral potentials applied in this thesis, we use $\Lambda = 500$ MeV [56].

Chapter 4

Relevance of contact terms *versus* pion exchanges in lower partial waves

In Ref. [56], NN potentials through all orders from LΩ to N^{4}LΩ were constructed. There are improvements in the reproduction of the empirical phase shifts as the orders increase and an excellent agreement is achieved at orders N^{3}LΩ and N^{4}LΩ. More similar results, one can see in Ref. [62–65]. In Fig 4.1, we display the phase shifts up to D-waves. Note that these fits involve two contacts at LΩ which contribute in S-waves, nine contacts at NLΩ and NNLΩ which contribute up to P-waves, and 24 contacts at N^{3}LΩ and N^{4}LΩ which contribute up to D-waves [cf. Eq. (3.49)]. The purpose of this chapter is to analyze in detail the role of these contacts in the fits of the $L \leq 2$ phase shifts up to N^{3}LΩ.

As discussed, the nuclear force consists essentially of two parts: the short range (Sect. 3.4) and the long range (Sect. 3.3). In chiral EFT, the long-range is represented by one- and multi-pion exchanges, and the short range is described by contact terms. The lower partial waves are particularly sensitive to the short range and, in fact, at N^{3}LΩ, four contact terms contribute to each S-waves, two to each P-waves, and one to each D-waves [cf. Eq. (3.49)]. There are no contact contributions in F and higher partial waves—at N^{3}LΩ.

Since lower partial waves are more sensitive to the short range potential, one may suspect that the contact contributions are dominant and simply override the pion-exchange contributions in lower partial waves which, on the other hand, are the most important ones in applications of the potentials to nuclear structure and reactions.

Consequently, in Ref. [48], only F and higher partial waves were used to show the effect of pion-contributions up to N^{4}LΩ and in Ref. [49] the same was done for G and higher partial waves to demonstrate chiral contributions up to N^{5}LΩ.

On the other hand, in applications of NN-potentials to nuclear structure and reactions, only the lower partial waves make large contributions. Thus, if chiral symmetry rules only the higher partial waves while the lower partial wave are essentially governed by

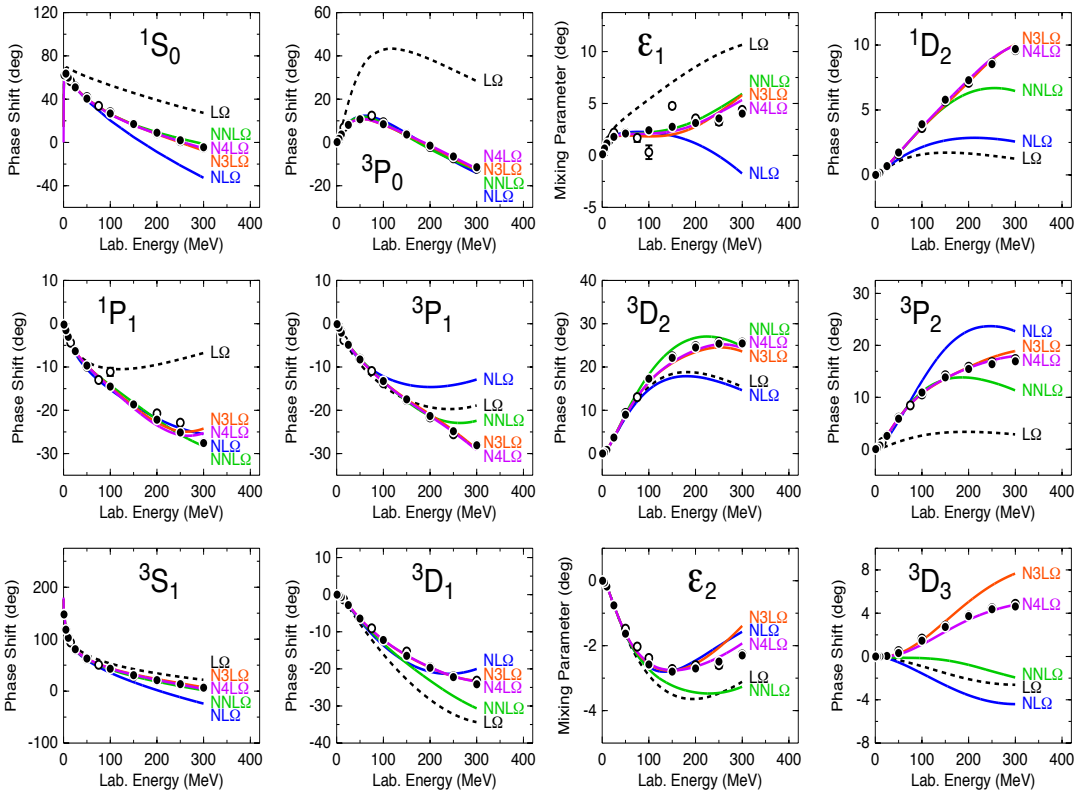

Figure 4.1: Chiral expansion of np scattering as represented by the phase shifts in S, P, and D-waves and mixing parameters ϵ_1 and ϵ_2. Five orders ranging from LΩ to N^{4}LΩ are shown as denoted. The solid dots and open circles are results from the Nijmegen multi-energy np phase shift analysis [36] and GWU single-energy np analysis [66], respectively. (From Ref. [56])

Table 4.1: Values of the πN low-energy constants (LECs) as determined in Ref. [67]. The c_i and $\bar{d}_i$ are the LECs of the second and third order πN Lagrangians, Eq. (2.13), and are in units of GeV^{-1} and GeV^{-2}, respectively. The uncertainties in the last digit are given in parentheses after the value.

	NNLΩ	$\mathrm{N^3LO}$
c_1	-0.74(2)	-1.07(2)
c_2		3.20(3)
c_3	-3.61(5)	-5.32(5)
c_4	2.44(3)	3.56(3)
$\bar{d}_1 + \bar{d}_2$		1.04(6)
$\bar{d}_3$		-0.48(2)
$\bar{d}_5$		0.14(5)
$\bar{d}_{14} - \bar{d}_{15}$		-1.90(6)

the contacts, then the predictions from these "chiral" potentials for nuclear structure and reactions would have little to do with chiral symmetry.

Motivated by the above concerns, the purpose of this study is to systematically investigate the role of those contacts versus pion exchange in those lower partial waves of NN scattering.

In our NN potential construction, the πN LECs are not fit-parameters; they are held fixed at their values determined in πN scattering [67] shown in Table 4.1. Therefore, the LECs of the NN contacts are the only fit parameters available to optimize the reproduction of the NN data (below 300 MeV laboratory energy). In this investigation, we will use the contact LECs to fit specific NN low-energy parameters or phase shifts. We will consider various scenarios, namely, using contacts only or using contacts together with pion contributions of increasing chiral order. The failure to reproduce the NN data by contacts only and the improvements that occur when (chiral) pion contributions are added will reveal the relevance of chiral symmetry in those lower partial waves. To obtain maximum insight into the role that contact terms can play, we will not follow here the rule that contact and pion contributions should be of the same order. In fact, we may, for example, consider contact contributions up to fourth order alone or with just the (lowest

order) 1PE or low-order 2PE added, to demonstrate what contacts can maximally achieve or not achieve. For contacts and pion exchanges, we consider orders up to $N^3LΩ$ (fourth order).

To keep it simple at the start, we begin with the partial waves that have only one contact, namely, D-waves and, then, proceed to the more elaborate cases, P and S-waves.

4.1 D-waves

To demonstrate the relevance of the pion exchange contributions (*versus* contacts) in D-waves, we consider the following cases for which we introduce the short notation given in parenthesis.

- Contact contribution only (ct1).
- LΩ pion exchange (i. e., 1PE) only and no contact term (L0).
- LΩ 1PE plus contact term (L1).
- NLΩ pion exchanges only, no contact term (NL0).
- NLΩ pion exchanges plus contact term (NL1).
- NNLΩ pion exchanges only, no contact term (NNL0).
- NNLΩ pion exchanges plus contact term (NNL1).
- $N^3LΩ$ pion exchanges plus contact term (NNNL1).

Our short notation (given in parenthesis) is designed such that the letters indicate the order of the pion exchanges included and the integer states the number of contacts involved (from the contacts available for the given partial wave). Note that in D-waves, there is only one (fourth order) contact per partial wave available, Eq. (3.49). When we include this contact term, we fit it to the empirical phase-shift at 50 MeV laboratory energy as

Table 4.2: Contact LECs used for D-waves [cf. Eq. (3.49)] in units of 10^4 GeV^{-6}.

case	$D_{^1D_2}$	$D_{^3D_2}$	$D_{^3D_3}$
ct1	-3.2575	-5.7202	-1.0130
L1	-1.6165	-0.0578	-1.7843
NL1	-1.2045	-0.3464	-2.3773
NNL1	-0.2068	0.2023	-1.3345
NNNL1	-2.088	-3.3804	-1.4764

determined in the Nijmegen phase-shift analysis [36]. The values for the contact LECs so obtained are listed in Table 4.2.

Note that the chiral 2PE expressions at orders NLΩ, Eqs. (3.20) and (3.21), and NNLΩ, Eqs. (3.24) and (3.25), include polynomial terms of order Q^2 [47], which do not contribute in D-waves [cf. Eq. (3.52) and text below the equation]. Therefore, in the cases of L1, NL1, and NNL1, the Q^4 contacts are not renormalized and represent the true corrections needed on top of the non-polynomial parts of the pion-exchanges, denoted by L0, NL0, and NNL0, respectively, in Fig. 4.2.

The situation is different at N^{3}LΩ. The subtracted dispersion integrals, Eq. (3.33), generate—besides the non-polynomial parts—also contact contributions up to fourth order. Moreover, the other N^{3}LΩ 2PE contributions also include polynomial terms of $\mathcal{O}(Q^4)$. Thus, the fourth order contact term we introduce to fit the phase shift at 50 MeV, includes a compensation for the fourth order polynomial terms generated by the N^{3}LΩ 2PE contributions. Therefore, in the case of NNNL1 of Table 4.2, the contact LEC is "renormalized", and it is not just the correction needed besides the genuine 2PE contributions. In fact, the large size of the NNNL1 contact LECs shown in Table 4.2 indicate that the fourth order polynomial terms generated by N^{3}LΩ pion contributions can be sizable.

The phase shifts up to 300 MeV predicted for the various cases are shown in Fig. 4.2. Next we will discuss those phase shifts partial wave by partial wave.

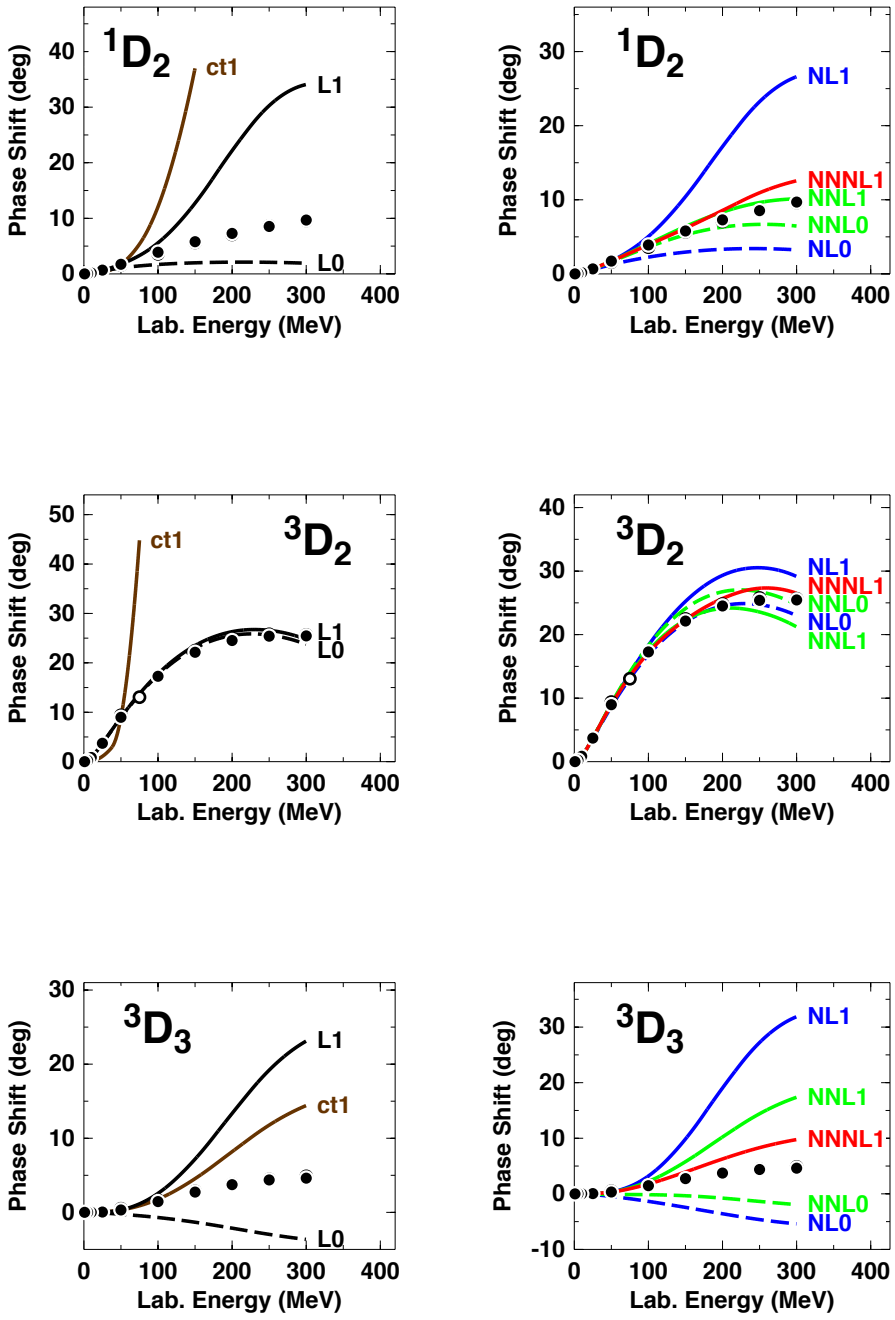

Figure 4.2: D-wave phase shifts of neutron-proton scattering for the various cases discussed in the text. Solid dots and open circles as in Fig. 4.1.

4.1.1 The $^1D_2$-wave

We start with the left $^1D_2$ frame in Fig. 4.2. When only the contact term is applied and no pion-exchanges (curve ct1) then the phase shift increases dramatically with energy indicating that the contact contribution is of very short range and completely inadequate to describe this D-wave. 1PE is weak (curve L0). Adding the contact to 1PE brings the phase shift up, but too much since obviously the contact is dominant. When 2PE contributions are added (right $^1D_2$ frame), the description improves with increasing order. While the NLΩ 2PE is weak and, therefore, does not lead to much improvement (cf. NL0 and NL1), the NNLΩ 2PE is known to provide a realistic intermediate-range attraction and together with the contact leads to a quantitative description (curve NNL1), and so does NNNL1. The conclusion is that the contact alone can by no means describe $^1D_2$. The strong intermediate-range attraction provided by chiral 2PE at NNLΩ and N^{3}LΩ is crucial. As the small contact LEC in the case of NNL1 reveals (Table 4.2), the contact contribution is minor, while chiral 2PE rules. This example demonstrates that even when a contact term is involved, chirality is still the major factor and shows its clear signature.

4.1.2 The $^3D_2$-wave

Also in this case, the contact contribution alone (cf. ct1 curve in the left $^3D_2$ frame in Fig. 4.2) leads to a dramatically wrong description. In this particular partial wave, the 1PE (L0 curve) happens to play a dominant role, because the matrix element of the tensor operator is 2 in this state which, in addition, is multiplied by (-3) from the $\boldsymbol{\tau}_1 \cdot \boldsymbol{\tau}_2$ factor, resulting in an overall factor of (-6) for the pion tensor potential. As the L0 curve reveals, this large tensor contribution alone, essentially, explains the $^3D_2$-wave. 2PE contributions play only a minor role (cf. right $^3D_2$ frame), because the (mainly) central forces provided by 2PE are small as compared to the huge tensor force contribution from 1PE in this particular wave. This scenario leaves little room for contact contributions. One-pion-exchange, the most pronounced expression of chiral symmetry, rules this wave.

4.1.3 The $^3D_3$-wave

The cases ct1, L0, and L1 are inadequate similarly to what we have seen in $^1D_2$. The 2PE contributions at NLΩ and NNLΩ without and with contact contribution (NL0, NNL0 and NL1, NNL1, respectively) do not lead to much improvement. Finally, with NNNL1 a more realistic result starts to develop. A quantitative description has to wait for N^{4}LΩ as demonstrated in the $^3D_3$ frame of Fig. 4.1. In any case, the contact alone cannot describe the $^3D_3$ wave, since the contact contribution is too short-ranged. Substantial intermediate-range attraction is needed, which only chiral 2PE can provide.

4.1.4 The $^3D_1$-wave

Since the $^3D_1$ wave is coupled to $^3S_1$, it will be discussed in conjunction with the coupled $^3S_1$-$^3D_1$ system, below.

4.1.5 D-wave summary

Contacts alone can not reproduce D-waves (cf. all the ct1 cases in the left column of Fig. 4.2), because of the short-range nature of the contact contributions, which is ill-suited for D-waves. The strong intermediate-range attraction provided by chiral 2PE at NNLΩ and N^{3}LΩ is crucial, unless the 1PE tensor force is dominant, which also is a reflection of chiral symmetry. For exact fits, contact corrections are needed, but they are very small. Thus, in spite of contributions from contacts, chirality makes the largest imprint on D-waves.

The D-waves are, in fact, an interesting case. On the one hand, they are not so peripheral that the (very long-ranged) 1PE is dominant and, on the other hand, their orbital angular momentum is large enough to prevent them from being too sensitive to the (short-ranged) contact potential. Thus, the D-waves are a true window on the intermediate range. Consequently, they test the reality of the (intermediate-ranged) 2PE as produced by chiral symmetry. In particular, the $^1D_2$-wave demonstrates that this test is passed well.

4.2 P-waves

In P-waves, we have two contacts available per partial wave; one is of order two, C_α, and the other one is of order four, D_α [cf. Eq. (3.49)]. We then consider the following cases with the short notation given in parenthesis.

- One contact contribution and nothing else (ct1).
- Two contact contributions (ct2).
- LΩ pion exchange (i. e., 1PE) only and no contact term (L0).
- LΩ 1PE plus one contact term (L1).
- LΩ 1PE plus two contact terms (L2).

- NLΩ pion exchanges plus one contact term (NL1).
- NLΩ pion exchanges plus two contact terms (NL2).
- NNLΩ pion exchanges plus one contact term (NNL1).
- NNLΩ pion exchanges plus two contact terms (NNL2).
- $N^3LΩ$ pion exchanges plus two contact terms (NNNL2).

The values for the contact LECs used in the various cases are listed in Table 4.3.

As mentioned, the chiral 2PE expressions at orders NLΩ and NNLΩ include polynomial terms of order Q^2 and the 2PE expressions at order $N^3LΩ$ include polynomial terms up to order Q^4. $\mathcal{O}(Q^2)$ and $\mathcal{O}(Q^4)$ polynomial terms do not vanish in P-waves [Eq. (3.52)]. These terms are absorbed by the second and fourth order contact terms. Therefore, the minimal number of contacts to be applied at NLΩ and NNLΩ is one (second order) contact and two (second and fourth order) contacts at $N^3LΩ$. Thus, the contact LECs shown in Table 4.3 for NL1, NNL1, and NNNL2 are not just the corrections needed besides the genuine 2PE contributions and their size does not reflect the size of "what is missing". However, in the cases NL2 and NNL2, the second contact included, D_α (fourth order contact), is not renormalized (since NLΩ and NNLΩ 2PE does not generate Q^4 polynomials) and, therfore, reflects a true fourth order correction.

The phase shifts up to 300 MeV that result from the various P-wave cases are shown in Fig. 4.3, which we will discuss now.

When we apply only one contact, we use the contact of second order and fit it to the empirical phase-shift at 50 MeV laboratory energy as determined in the Nijmegen phase-shift analysis [36]. When both contacts are involved, we fit the empirical phase-shifts at 50 MeV and 150 MeV (if possible).

Obviously, with just one contact term and no pion contributions (cases ct1 of the left column of Fig. 4.3) the description is grossly wrong in all P-waves. Adding the second

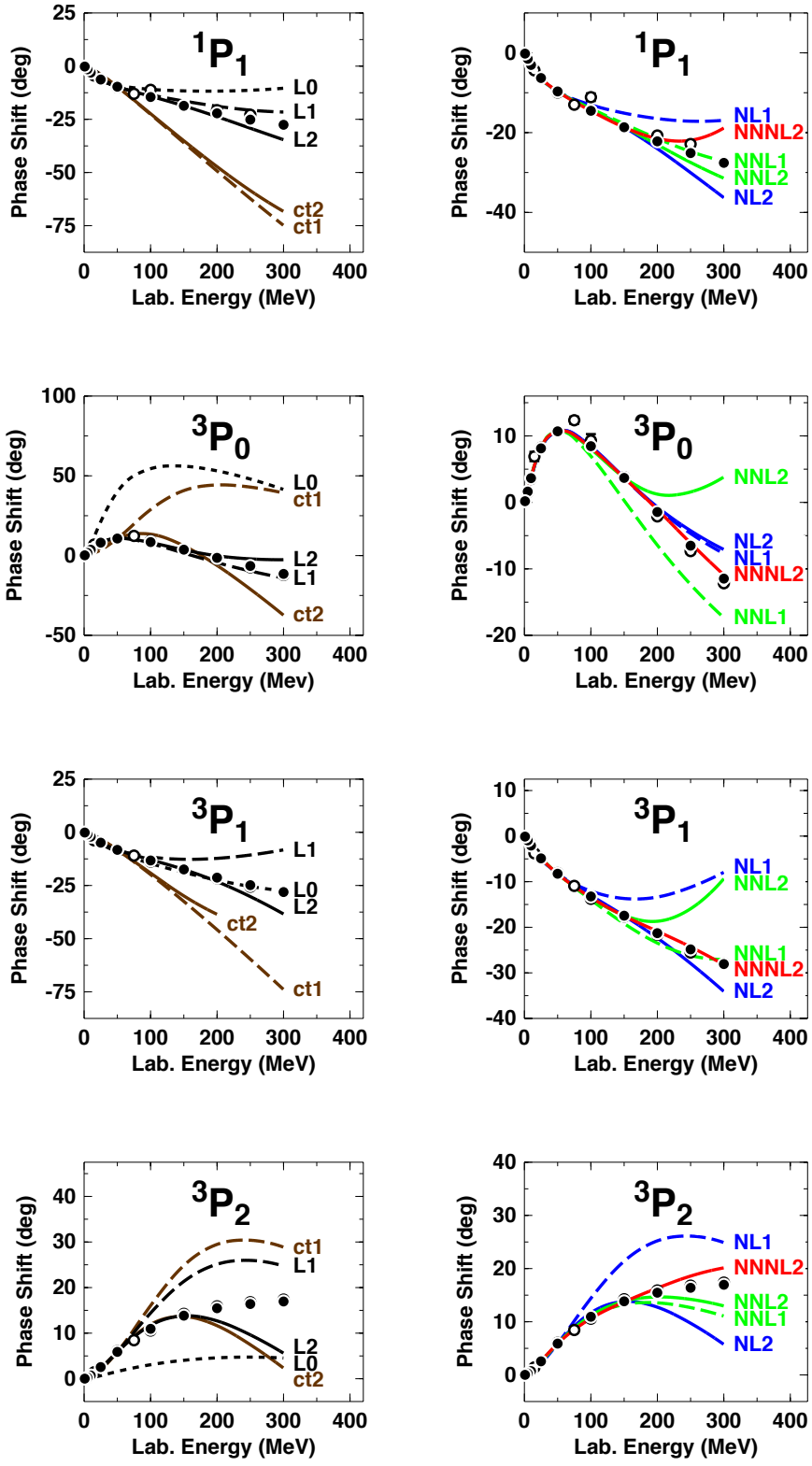

Figure 4.3: P-wave phase shifts of neutron-proton scattering for the various cases discussed in the text. Solid dots and open circles as in Fig. 4.1.

Table 4.3: Contact LECs used in P-waves [cf. Eq. (3.49)]. Second order contacts, C_α, are in units of 10^4 GeV^{-4}, while fourth order contacts, D_α, are in units of 10^4 GeV^{-6}.

	$^1P_1$		$^3P_0$		$^3P_1$		$^3P_2$	
case	$C_{^1P_1}$	$D_{^1P_1}$	$C_{^3P_0}$	$D_{^3P_0}$	$C_{^3P_1}$	$D_{^3P_1}$	$C_{^3P_2}$	$D_{^3P_2}$
ct1	6.5533	0	-0.4631	0	4.3248	0	-0.3256	0
ct2	2.17	-5.0	-0.874	10.0	1.4127	-5.0	-0.4766	1.6
L1	0.1349	0	0.8463	0	-0.1732	0	-0.2302	0
L2	0.1613	0.95	0.8531	-0.55	-0.1480	1.58	-0.3300	1.1
NL1	0.2295	0	1.3228	0	-0.4607	0	-0.2203	0
NL2	0.2664	1.45	1.3234	-0.03	-0.4352	1.2	-0.3203	1.1
NNL1	0.1821	0	1.1415	0	-0.7851	0	-0.6333	0
NNL2	0.1912	0.3	1.1495	-0.95	-0.8133	-0.58	-0.6251	-0.1
NNNL2	0.1933	9.72	1.1883	4.92	-0.8105	4.74	-0.7464	5.95

contact does not lead to any improvement in $^1P_1$ and $^3P_1$ and, in fact, in these two cases it is not possible to fit the phase shift at 150 MeV, in spite of the second term. The $^3P_0$ and $^3P_2$ partial waves improve with the second contact, but are not any close to a quantitative description. Adding 1PE (L0) together with one or two contacts (L1, L2) brings about considerable improvement in most P-waves. Turning to the frames of the right column of Fig. 4.3 where the 2PE exchanges of various orders are added, we observe order by order improvement. $^1P_1$ is described well in the cases of NNL1 and NNL2, while the other partial waves assume a quantitative character only when the powerful 2PE at N^{3}LΩ is added (case NNNL2).

In summary, contacts alone are inadequate to describe P-waves. 1PE brings improvement, but strong chiral 2PE is needed for a quantitative description of P-waves. Thus, a clear signature of chiral symmetry can be identified in P-waves.

A note is in place on $^3P_2$, since it is coupled with $^3F_2$ and ϵ_2 through the contact LEC $D_{^3P_2-^3F_2}$, Eq. (3.49). We found that the latter parameter has only a weak effect on the $^3P_2$ phase shift and, therefore, we decided to leave it out of our considerations. We kept it at zero.

Table 4.4: Columns two to five show the contact LECs used in the $^1S_0$ wave [cf. Eq. (3.49)]. The zeroth order contact $\widetilde{C}_{^1S_0}$ is in units of 10^4 GeV^{-2}; the second order contact $C_{^1S_0}$ in units of 10^4 GeV^{-4}; and fourth order contacts $\widehat{D}_{^1S_0}$ and $D_{^1S_0}$ in units of 10^4 GeV^{-6}. Column six and seven display the np scattering length, a_{np}, and effective range, r_{np}, in the $^1S_0$ state.

case	$\widetilde{C}_{^1S_0}$	$C_{^1S_0}$	$\widehat{D}_{^1S_0}$	$D_{^1S_0}$	a_{np} (fm)	r_{np} (fm)
ct1	-0.063985	0	0	0	-23.74	0.69
ct2	0.475799	4.0	0	0	-23.74	2.37
ct3	-0.158301	2.0	-6.0	0	-23.74	2.66
L1	-0.109340	0	0	0	-23.74	1.73
L2	-0.130919	1.33	0	0	-23.74	2.70
NL2	-0.146214	1.815	0	0	-23.74	2.70
NNL2	-0.152032	2.36	0	0	-23.74	2.70
NNNL4	-0.139563	2.417	-2.332	-16.74	-23.74	2.70

4.3 The $^1S_0$-wave

In the $^1S_0$ wave, we have available a total of four contact terms [cf. Eq. (3.49)], namely, one zeroth order contact, $\widetilde{C}_{^1S_0}$, one second order contact, $C_{^1S_0}$, and two fourth order contacts, $\widehat{D}_{^1S_0}$ and $D_{^1S_0}$. When we use only one contact, we pick the zeroth order one and fit it to the np $^1S_0$ scattering length, $a_{np} = -23.74$ MeV. When we apply two contacts, we fit, besides the scattering length, the $^1S_0$ np effective range parameter, $r_{np} = 2.70 \pm 0.05$ MeV.

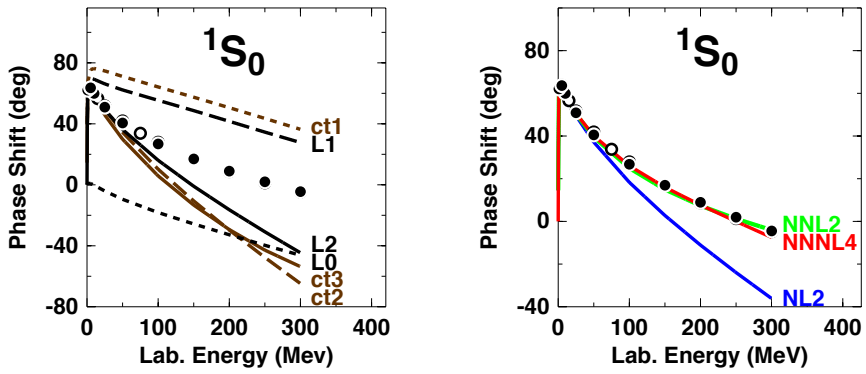

Figure 4.4: $^1S_0$ phase shifts of neutron-proton scattering for the various cases discussed in the text. Solid dots and open circles as in Fig. 4.1.

With three parameters, we also try to reproduce (if possible) the empirical phase-shift at 50 MeV laboratory energy as determined in the Nijmegen phase-shift analysis [36] and, with four parameters, the phase shift at 150 MeV is included in the fit. We consider the following cases with the short notation given in parenthesis.

- One contact contribution, and nothing else (ct1).
- Two contact contributions (ct2).
- Three contact contributions (ct3).
- LΩ 1PE and no contact term (L0).
- LΩ 1PE plus one contact term (L1).
- LΩ 1PE plus two contact terms (L2).
- NLΩ pion exchanges plus two contact terms (NL2).
- NNLΩ pion exchanges plus two contact terms (NNL2).
- N^3LΩ pion exchanges plus four contact terms (NNNL4).

The values for the contact LECs are listed in Table 4.4 and the phase shifts up to 300 MeV that result from the various $^1S_0$ cases are shown in Fig. 4.4, which we will discuss now.

When only one contact term is used (fit to a_{np}) and no pion contributions (case ct1), then the $^1S_0$ phase shifts are far above the data. Adding more contacts (cases ct2 and ct3) moves the predictions far below the data. The prediction with four contacts is essentially the same as with three contacts and, therefore, not shown. Clearly, contacts alone cannot describe the $^1S_0$ wave, no matter how many contacts one is using. 1PE alone (L0) is small and adding to it one or two contacts (cases L1 and L2) brings about predictions that are very similar to the corresponding cases with contacts alone (ct1 and ct2) and,

again, adding more contacts does essentially not change anything. Thus, in $^1S_0$, 1PE is obviously of very limited relevance, except for the effective range parameter, r_{np}, which is improved by 1PE (cf. Table 4.4). The strong part of 1PE is its tensor force, which does not contribute in singlet states where only the (weak) central force has a presence. The momentum-space 1PE includes also a constant term/contact term [see Eq. (3.14)], which converts into a $\delta(\vec{r})$-function in position space. The L0 case includes the $\delta(\vec{r})$-function contribution.

We now turn to the frame on the right of Fig. 4.4, where the 2PE exchanges of the various orders are added in. The NLΩ 2PE (curve NL2) does not create any improvement over the L2 case. However 2PE at NNLΩ (curve NNL2) leads to an excellent reproduction of the $^1S_0$ phase shifts up to 300 MeV. Adding more contacts beyond two in the cases of NLΩ and NNLΩ does not improve the description, which is why we do not show these cases. The NNNL4 case creates further subtle refinements.

We remind the reader again of the fact that the chiral 2PE expressions at orders NLΩ and NNLΩ include polynomial terms of order Q^0 and Q^2, and the 2PE expressions at order N^{3}LΩ include polynomial terms up to order Q^4, which are always compensated by contacts of the same order. Therefore, in the case of the $^1S_0$ wave, the minimal number of contacts to be applied at NLΩ and NNLΩ is two (zeroth and second order) and four (of orders zero, two, and four) at N^{3}LΩ. Thus, the contact LECs shown in Table 4.4 for NL2, NNL2, and NNNL4 are renormalized numbers whose size does not necessarily reflect the size of what is missing beyond the genuine pion exchange contributions.

In summary, contacts alone are inadequate to describe the $^1S_0$-wave. The strong chiral 2PE that starts at NNLΩ is needed for a quantitative description of the $^1S_0$-wave. There is a clear signature of chiral symmetry in $^1S_0$-wave.

Table 4.5: Columns two to seven show the contact LECs used in the ${}^3S_1 - {}^3D_1$ waves [cf. Eq. (3.49)]. The $\widetilde{C}_\alpha$ of the zeroth order contact are given in units of 10^4 GeV^{-2}; the C_α of second order in 10^4 GeV^{-4}; and $\widehat{D}_\alpha$ and D_α of fourth order in 10^4 GeV^{-6}. Column eight and nine display the triplet scattering length, a_t, and effective range, r_t, respectively, in the ${}^3S_1$ state.

case	$\widetilde{C}_{^3S_1}$	$C_{^3S_1}$	$\widehat{D}_{^3S_1}$	$D_{^3S_1}$	$D_{^3D_1}$	$C_{^3S_1-{}^3D_1}$	a_t (fm)	r_t (fm)
ct1	-0.077103	0	0	0	0	0	5.42	0.68
ct5	-0.1311	2.0	-0.5	0	27.0	-1.25	5.42	1.76
L1	-0.06366	0	0	0	0	0	5.42	1.59
L5	-0.13345	0.4	-0.7	0	-2.0	0.41	5.42	1.73
NL2	-0.136835	-0.39	0	0	0	0	5.42	1.76
NL5	-0.1255	-0.5	-2.3	0	-2.3	0.1	5.42	1.73
NNL2	-0.10002	-0.335	0	0	0	0	5.42	1.75
NNL5	-0.14875	0.4	-0.1	0	-1.4	0.4	5.42	1.74
NNNL8[a]	-0.159635	0.8233	-4.319	-19.17	-5.59	0.503	5.42	1.75

[a] In the case of NNNL8, besides the six parameters given, $\widehat{D}_{^3S_1-{}^3D_1} = 1.162$ and $D_{^3S_1-{}^3D_1} = 1.759$. In all other cases, $\widehat{D}_{^3S_1-{}^3D_1} = D_{^3S_1-{}^3D_1} = 0$.

4.4 The coupled ${}^3S_1$-${}^3D_1$ system

In the coupled ${}^3S_1$-${}^3D_1$ system, we have available a total of eight contact terms [cf. Eq. (3.49)]; namely, four for ${}^3S_1$ ($\widetilde{C}_{^3S_1}$, $C_{^3S_1}$, $\widehat{D}_{^3S_1}$, $D_{^3S_1}$), one for ${}^3D_1$ ($D_{^3D_1}$), and three for the ${}^3S_1$-${}^3D_1$ transition potential ($C_{^3S_1-{}^3D_1}$, $\widehat{D}_{^3S_1-{}^3D_1}$, $D_{^3S_1-{}^3D_1}$). When we use only one of the eight contacts, we pick the zeroth order one, $\widetilde{C}_{^3S_1}$, and fit it to the ${}^3S_1$ scattering length, $a_t = 5.42$ MeV. When we apply the two contacts $\widetilde{C}_{^3S_1}$ and $C_{^3S_1}$, we fit, besides the scattering length, the ${}^3S_1$ effective range parameter, $r_t = 1.75 \pm 0.02$ MeV. Using the three ${}^3S_1$ parameters $\widetilde{C}_{^3S_1}$, $C_{^3S_1}$, and $\widehat{D}_{^3S_1}$, we try to also reproduce (if possible) the empirical ${}^3S_1$ phase-shift at 50 MeV laboratory energy as determined in the Nijmegen phase-shift analysis [36]. Besides the three contact LECs mentioned, we will, in some cases, also include $D_{^3D_1}$ and $C_{^3S_1-{}^3D_1}$, which affect the $3D_1$ phase shift and the ϵ_1 parameter, respectively. To prevent our investigation from becoming too involved, we do not vary the LECs $D_{^3S_1}$, $\widehat{D}_{^3S_1-{}^3D_1}$, and $D_{^3S_1-{}^3D_1}$ at orders up to NNLΩ and keep them

at zero. Thus, up to NNLΩ, we will be experimenting with maximally five contacts in the $^3S_1$-$^3D_1$ system.

We consider the following cases with the short notation given in parenthesis.

- One contact contribution, and nothing else (ct1).
- Five contact contributions (ct5).
- LΩ pion exchange (i. e., 1PE) plus one contact term (L1).
- LΩ 1PE plus five contact terms (L5).
- NLΩ pion exchanges plus two contact terms (NL2).
- NLΩ pion exchanges plus five contact terms (NL5).
- NNLΩ pion exchanges plus two contact terms (NNL2).
- NNLΩ pion exchanges plus five contact terms (NNL5).
- NNNLΩ pion exchanges plus eight contact terms (NNNL8).

The values for the contact LECs used in the various cases are listed in Table 4.5, and the corresponding phase shifts up to 300 MeV are shown in Fig. 4.5.

When only one contact term is used (fit to a_t) and no pion contributions (case ct1), then the $^3S_1$ phase shifts are substantially above the data and r_t is off by about 1 fm. Adding one more contact (cases ct2, not shown), gets r_t correct, but moves the phase shifts at intermediate energies far below the data, very similar to the case ct5 that is shown in Fig. 4.5. In fact, adding more contacts to the coupled system under consideration does not change the $^3S_1$ phase shifts up the maximum of five contacts. Clearly, contacts alone cannot describe the $^3S_1$ wave, no matter how many contacts one is using. However, adding 1PE (case L1) makes a big difference, getting the $^3S_1$ phase shifts almost right and finally perfect with more contacts (L5). This is quite in contrast to $^1S_0$, where 1PE has little

influence and where 1PE plus contacts never lead to a reproduction of the phase shifts. The reason for this is that, in the coupled ${}^3S_1$-${}^3D_1$ state, the 1PE tensor force contributes strongly which is crucial for the correct description of this coupled system.

We now turn to the ${}^3S_1$ frame on the right of Fig. 4.5, where the 2PE exchanges of the various orders are added, and we see that 2PE does not make much difference.

Turning to the ${}^3D_1$ phase shifts, we see again that contacts alone cannot get this partial wave right. The contact contribution is too short-ranged for this partial wave as clearly seen by the very small contribution at low energies and too strong a contribution above 150 MeV. Adding 1PE gets it right at low energies, but requires short-ranged corrections at higher energies. This can be done by contacts (case L5) or by 2PE contributions of higher order together with moderate contacts (right ${}^3D_1$ frame).

Finally, we turn to the ϵ_1 parameter, which is interesting, because it is proportional to the ${}^3S_1$-${}^3D_1$ transition potential created exclusively by the tensor force. 1PE generates a (too) strong tensor force (L1) which, when damped by a short ranged contact, gets it about right. The 2PE of the various orders do also generate more or less tensor force contributions which require short-range contact corrections to get it right.

Thus, qualitatively, 1PE plus a short-range correction is all that is needed for the ${}^3S_1$-${}^3D_1$ system. Interestingly, the chiral 2PE contributions are not important in this case. The deeper reason for this is that the iteration of the 1PE tensor force in this coupled system generates a 2PE contribution that is so strong that it makes other 2PE contributions insignificant.

We remind the reader again of the fact that the chiral 2PE expressions at orders NLΩ and NNLΩ include polynomial terms of order Q^0 and Q^2 and the 2PE expressions at order N^{3}LΩ include polynomial terms up to order Q^4. Therefore, in the case of the coupled ${}^3S_1$-${}^3D_1$ system, the minimal number of contacts to be applied at NLΩ and NNLΩ is three, namely, $\widetilde{C}_{{}^3S_1}$, $C_{{}^3S_1}$, and $C_{{}^3S_1-{}^3D_1}$. In the case of N^{3}LΩ it is eight.

In summary, contacts alone are inadequate to describe the ${}^3S_1$-${}^3D_1$ system. Crucial is the 1PE which, for good reasons, is called the *Leading Order* of the chiral expansion.

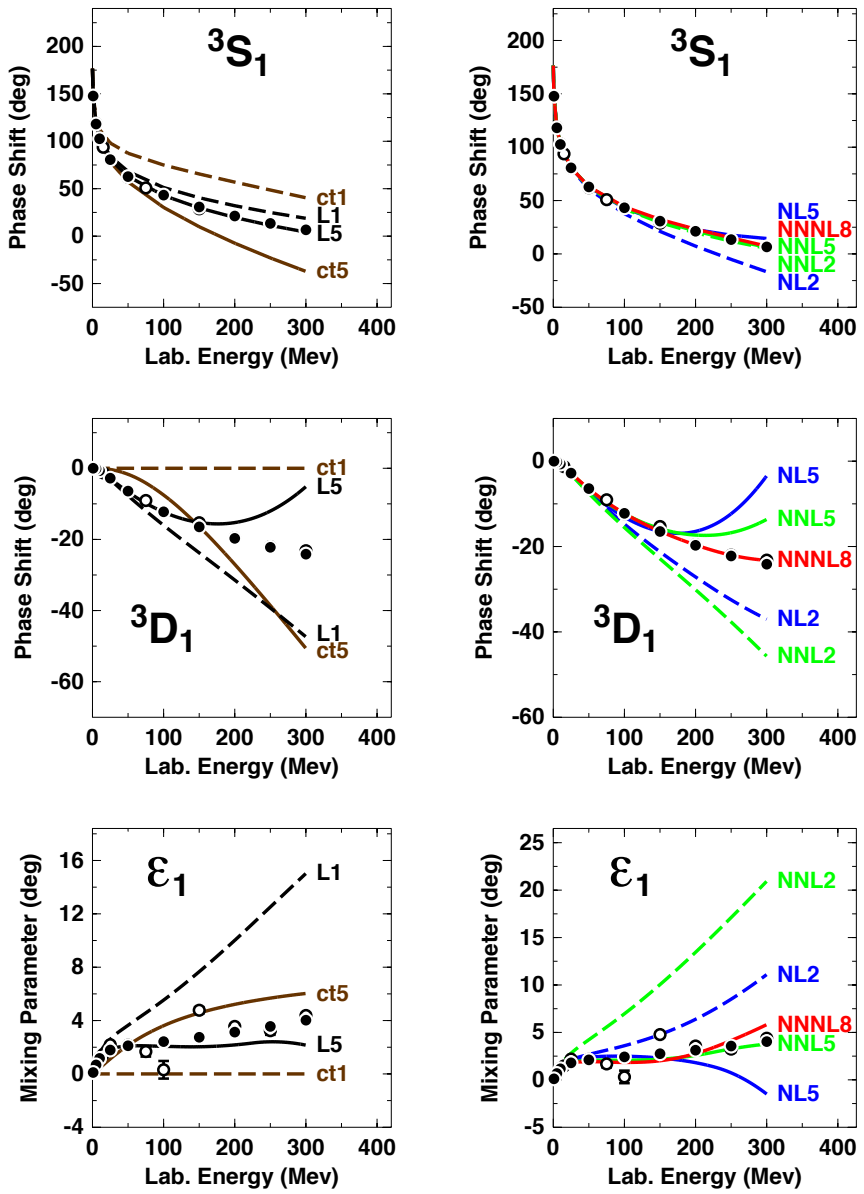

Figure 4.5: $^3S_1$, $^3D_1$, and ϵ_1 phase parameters of neutron-proton scattering for the various cases discussed in the text. Solid dots and open circles as in Fig. 4.1.

Chapter 5

Summary and conclusions

The most characteristic feature in the design of chiral NN potentials is that the long and intermediate-range part of the potential is described by one- and multi-pion exchanges which are ruled by chiral symmetry. In contrast, the short-range part consists simply of polynomial terms ("contact" terms), since the short-range nucleon structure cannot be resolved at low energies.

In the lower partial waves of NN scattering, which are the dominant ones for predictions of observable of nuclear structure and reactions, contacts as well as pion-exchanges contribute. But, since lower waves are presumed to be more sensitive to the short-range, one may suspect that the contact terms are dominant and simply override the (chiral) pion-exchange contributions.

Motivated by the above concerns, the purpose of this thesis was to systematically investigate the role of the contacts, on the one hand, and the effect of the pion exchanges, on the other hand, in the lower partial waves of chiral NN potentials.

We have shown in detail what contact terms alone can achieve in the lower partial waves of NN scattering. This is displayed by the brown ct curves in the left frames of Figs. 4.2 to 4.5, which all demonstrate that contacts alone are totally inadequate and do not catch anything of the nature of the nuclear force in those partial waves. Adding (chiral) 1PE yields semi-realistic results in some specific partial-wave states, where the tensor force plays an outstanding role. Such cases are the ${}^3D_2$ state and the ${}^3S_1$-${}^3D_1$ system that is coupled through the tensor force. Chiral 2PE at NLΩ is generally weak and, therefore, does not bring about much improvement. However, the NNLΩ 2PE is very strong, creating a realistic intermediate range attraction that cannot be simulated by contacts.

This fact is also reflected in the χ^2 calculations for the fit of the NN data conducted in Ref. [56]. While the χ^2/datum at NLΩ comes out to be 51.5, at NNLΩ it is 6.3, even

though in both cases the number of contact terms is the same. The improvement in the χ^2 is due to an improvement of the chiral 2PE at NNLΩ. Obviously, the contacts cannot substitute the chiral terms.

In conclusion, despite the fact that contact and pion-exchange contributions are entangled in the all important lower partial waves of an NN potential, we were able to disentangle them. We managed to identify and pin down many characteristic signatures of chiral symmetry that are crucial for the quantitative description of the nuclear force in those low angular momentum states. However, that does not imply that contacts are totally useless. For the accurate fit of NN quantities like the effective range parameters, the phase shifts at low energies, and the deuteron binding energy, contacts are needed. They play a subtle role and are like the "dot over the i".

Appendix A: The hierarchy of nuclear forces: Overview

Leading order (LO, ν=0)

At LO, we have only two contact contributions with no momentum dependence ($\sim Q^0$), represented by the four-nucleon-leg diagram with a small-dot vertex shown in the first row of Fig. 3.1. Furthermore, we have the static one-pion exchange (1PE), represented by the second diagram of the first row of Fig. 3.1.

This description contains some of the main attributes of the NN force. First, the 1PE provides the tensor component of the force known to be crucial for the two-nucleon bound state. Second, it predicts correctly NN phase parameters for peripheral partial waves of very high orbital angular momentum. At this order, the two contacts, which contribute only in S-waves, provide the short- and intermediate-range interaction.

Note that in the next order, ν=1, all contributions vanish, as they would violate parity conservation and time-reversal invariance.

Next-to-leading order (NLO, ν=2)

The two-pion exchange (2PE) occurs for the first time at this order, and thus it is referred to as the leading 2PE. This contribution is essential for a realistic account of the intermediate-range attraction. However, the leading 2PE has insufficient strength, for the following reason: the loops present in the 2PE diagrams which involve pions carry the power ν=2, and so only the lowest order πNN and $\pi\pi NN$ vertices with Δ_i=0 are allowed at this order, which is why these vertices are weak. Moreover, seven new contacts appear at this order which contribute in S and P waves. The two-nucleon contact terms are indicated by the four-nucleon-leg diagram with a solid square. At this power, the appropriate operators of these contacts include spin-orbit, central, spin-spin, and tensor terms, essentially all the spin operator structures needed for a realistic description of the 2NF, although the medium-range attraction still lacks sufficient strength.

Next-to-next-to-leading order (NNLO, ν=3)

The 2PE contains now the two-derivative $\pi\pi NN$ seagull vertices denoted by a large solid dot. These vertices bring in correlated 2PE and intermediate $\Delta(1232)$-isobar contributions. No new contacts become available at this order, because contacts appear only at even orders. Three-nucleon forces appear at NLO, but their net contribution vanishes at this order. The first non-zero 3NF contribution is found here. It is therefore easy to understand why 3NF are very weak as compared to the 2NF which contributes already at $(Q/\Lambda)^0$.

Next-to-next-to-next-to leading order (N^{3}LO, ν=4)

We show a few representative diagrams in Fig. 3.1. There is a large attractive one-loop 2PE contribution (the bubble diagram with two large solid dots), which slightly overestimates the 2NF attraction at medium range. Two-pion-exchange graphs with two loops are seen at this order, together with three-pion exchange (3PE), which was determined to be very weak at N^{3}LO. Most importantly, 15 new additional contacts $\sim Q^4$ arise at this order, signified by the four-nucleon-leg diagram in the figure with the diamond-shaped vertex. These contacts impact states with orbital angular momentum up to $L = 2$ (D-waves), and are the reason for the quantitative description of the two-nucleon force at this order. More 3NF diagrams show up at N^{3}LO, as well as the first contributions to four-nucleon forces (4NF). The investigation of this paper is carried out up to N^{3}LO.

Appendix B: Contacts in terms of partial waves

The zeroth-order (leading order, LO), contacts, Eq. (3.46), are given in terms of partial waves by

$$V_{ct}^{(0)}({}^1S_0) = \tilde{C}_{{}^1S_0} = 4\pi\,(C_S - 3C_T), \tag{1}$$

$$V_{ct}^{(0)}({}^3S_0) = \tilde{C}_{{}^3S_0} = 4\pi\,(C_S + C_T). \tag{2}$$

The second order (NLO) contacts, Eq. (3.47), lead to the following partial-wave contributions:

$$\begin{aligned}
V_{ct}^{(2)}({}^1S_0) &= C_{{}^1S_0}(p^2 + p'^2),\\
V_{ct}^{(2)}({}^3P_0) &= C_{{}^3P_0}\,pp',\\
V_{ct}^{(2)}({}^1P_1) &= C_{{}^1P_1}\,pp',\\
V_{ct}^{(2)}({}^3P_1) &= C_{{}^3P_1}\,pp',\\
V_{ct}^{(2)}({}^3S_1) &= C_{{}^3S_1}(p^2 + p'^2),\\
V_{ct}^{(2)}({}^3S_1 - {}^3D_1) &= C_{{}^3S_1-{}^3D_1}p^2,\\
V_{ct}^{(2)}({}^3D_1 - {}^3S_1) &= C_{{}^3S_1-{}^3D_1}p'^2,\\
V_{ct}^{(2)}({}^3P_2) &= C_{{}^3P_2}\,pp'.
\end{aligned} \tag{3}$$

The relationship between the $C_{(2s+1)_{L_J}}$ and the C_i can be found in Ref. [41].

The fourth-order (N^3LO) contacts, Eq. (3.48), after partial-wave decomposition, are

represented by [41]:

$$
\begin{aligned}
V_{ct}^{(4)}({}^1S_0) &= \widehat{D}_{{}^1S_0}(p'^4+p^4) + D_{{}^1S_0}p'^2p^2,\\
V_{ct}^{(4)}({}^3P_0) &= D_{{}^3p_0}(p'^3p+p'p^3),\\
V_{ct}^{(4)}({}^1P_1) &= D_{{}^1p_1}(p'^3p+p'p^3),\\
V_{ct}^{(4)}({}^3P_1) &= D_{{}^3p_1}(p'^3p+p'p^3),\\
V_{ct}^{(4)}({}^3S_1) &= \widehat{D}_{{}^3S_1}(p'^4+p^4) + D_{{}^3S_1}p'^2p^2,\\
V_{ct}^{(4)}({}^3D_1) &= D_{{}^3D_1}p'^2p^2,\\
V_{ct}^{(4)}({}^3S_1-{}^3D_1) &= \widehat{D}_{{}^3S_1-{}^3D_1}p^4 + D_{{}^3S_1-{}^3D_1}p'^2p^2,\\
V_{ct}^{(4)}({}^3D_1-{}^3S_1) &= \widehat{D}_{{}^3S_1-{}^3D_1}p'^4 + D_{{}^3S_1-{}^3D_1}p'^2p^2,\\
V_{ct}^{(4)}({}^1D_2) &= D_{{}^1D_2}p'^2p^2,\\
V_{ct}^{(4)}({}^3D_2) &= D_{{}^3D_2}p'^2p^2,\\
V_{ct}^{(4)}({}^3P_2) &= D_{{}^3p_2}(p'^3p+p'p^3),\\
V_{ct}^{(4)}({}^3P_2-{}^3F_2) &= D_{{}^3P_2-{}^3F_2}p'p^3,\\
V_{ct}^{(4)}({}^3F_2-{}^3P_2) &= D_{{}^3p_2-{}^3F_2}p'^3p,\\
V_{ct}^{(4)}({}^3D_3) &= D_{{}^3D_3}p'^2p^2. \qquad (4)
\end{aligned}
$$

The relationship between the $D_{(2s+1)_{L_J}}$ and the D_i is given in Ref. [41].

The full list of contributions for each partial-wave shown in Eq. (3.49) is assembled, order-by-order, from the partial-wave terms displayed in this Appendix.

Appendix C: The number of contact terms

Table C.1 shows that, at N^{3}LO, there are 24 parameters which impact partial waves with $L \leq 2$, while at NLO and NNLO there are only 9 contacts which contribute for $L \leq 1$. These LECs are free constants employed to parametrize the short-range phenomenology. Thus, at N^{3}LO, contacts appear for the first time in D-waves. This is one important mechanism behind the considerable improvement in the reproduction of the NN data at this order. Because the D-states are somewhat in between central and peripheral waves, contact terms, in addition to the one- and two-pion exchanges, are important to describe the D-phases correctly.

In the Table, we also show the number of parameters used in the Nijmegen partial wave analysis (PWA93) [36] and in the high-precision CD-Bonn potential [68]. The table reveals that, for S- and P-waves, the number of parameters used in high-precision phenomenology and in EFT at N^{3}LO are about the same. Thus, the EFT approach provides retroactively a justification for the phenomenology used in the 1990s to obtain high-precision fits. Consequently, at N^{3}LO, potentials can be constructed which are of about the same quality as the high-precision NN potentials of the 1990s.

Table C.1: Number of parameters needed for fitting the *np* data in the Nijmegen phase-shift analysis (Nijmegen PWA93 [36]) and by the high-precision CD-Bonn potential [68] versus the total number of NN contact terms of EFT-based potentials at different orders.

	Nijmegen PWA93	CD-Bonn	EFT		
			Q^0	Q^2	Q^4
$^1S_0$	3	4	1	2	4
$^3S_1$	3	4	1	2	4
$^3S_1$-$^3D_1$	2	2	0	1	3
$^1P_1$	3	3	0	1	2
$^3P_0$	3	2	0	1	2
$^3P_1$	2	2	0	1	2
$^3P_2$	3	3	0	1	2
$^3P_2$-$^3F_2$	2	1	0	0	1
$^1D_2$	2	3	0	0	1
$^3D_1$	2	1	0	0	1
$^3D_2$	2	2	0	0	1
$^3D_3$	1	2	0	0	1
$^3D_3$-$^3G_3$	1	0	0	0	0
$^1F_3$	1	1	0	0	0
$^3F_2$	1	2	0	0	0
$^3F_3$	1	2	0	0	0
$^3F_4$	2	1	0	0	0
$^3F_4$-$^3H_4$	0	0	0	0	0
$^1G_4$	1	0	0	0	0
$^3G_3$	0	1	0	0	0
$^3G_4$	0	1	0	0	0
$^3G_5$	0	1	0	0	0
Total	35	38	2	9	24

References

[1] E. Rutherford, Phil. Mag. **21**, 669 (1911).

[2] J. J. Thomson, Rays of Positive Electricity (Longmans Green New York, 1913).

[3] R. Machleidt, Adv. Nucl. Phys. **19**, 189-376 (1989).

[4] J. Chadwick, Proc. Roy. Soc. (London) **A136**, 692 (1932).

[5] E. Wigner, Phys. Rev. **43**, 252 (1933).

[6] W. Heisenberg, Z. Phys. **77**, 1 (1932).

[7] E. Majorana, Z. Phys. **82**, 137 (1933).

[8] J. Chadwick and M. Goldhaber, Nature **134**, 237 (1934).

[9] M. Tuve, N. Heydenburg, and L. Hafstad, Phys. Rev. **50**, 806 (1936).

[10] B. Cassen and E. U. Condon, Phys. Rev. **50**, 846 (1936).

[11] H. Yukawa, Proc. Phys. Math. Soc. (Japan) **17**, 48 (1935).

[12] A. Proca, J. Phys. Radium **7**, 347 (1936).

[13] N. Kemmer, Proc. Roy. Soc. **A166**, 127 (1938).

[14] J. Kellog, I. Rabi, N. F. Ramsey, and J. Zacharias, Phys. Rev. **55**, 318; **56**, 728 (1939).

[15] W. Pauli, Meson Theory of Nuclear Forces (Interscience, New York, 1946).

[16] G. P. S. Occhialini, C. F. Powell, C. M. G. Lattes, and H. Muirhead, Nature **159**, 694 (1947).

[17] C. M. C. Lattes, H. Muirhead, G. P. S. Occhialini, and C. F. Powell, Nature **159**, 694 (1947).

[18] G. Breit, Phys. Rev. **51**, 248 (1937).

[19] G. Breit and J. R. Stehn, Phys. Rev. **53**, 459 (1938).

[20] L. Rosenfeld, Nature **145**, 141 (1945).

[21] M. Taketani, S. Nakamura, and M. Sasaki, Prog. Theor. Phys. (Kyoto) **6**, 581 (1951).

[22] M. Taketani, S. Machida, and S. Ohnuma, Prog. Theor. Phys. **7**, 45 (1952).

[23] K. A. Brueckner and K. M. Watson, Phys. Rev. **90**, 699 (1953); **92**, 1023 (1953).

[24] K. A. Brueckner, M. Gell-Mann, and M. Goldberger, Phys. Rev. **90**, 476 (1953).

[25] A. R. Erwin, R. March, W. D. Walker, and E. West, Phys. Rev. Lett. **6**, 628 (1961).

[26] B. C. Maglić, L. W. Alvarez, A. H. Rosenfeld, and M. L. Stevenson, Phys. Rev. Lett. **7**, 178 (1961).

[27] R. A. Bryan and B. L. Scott, Phys. Rev. **135**, B434 (1964); **164**, 1215 (1967); **177**, 1435, (1969); and references therein.

[28] K. Holinde and R. Machleidt, Nucl. Phys. **A247**, 495 (1975).

[29] R. de Tourreil, B. Rouben, and D. W. L. Sprung, Nucl. Phys. **A242**, 445 (1975).

[30] M.M. Nagels, T. A. Rijken, and J. D. de Swart, Phys. Rev. **D17**, 768 (1978).

[31] M. Lacombe, B. Loiseau, J. M. Richard, R. V. Mau, J. Côté, P. Pirès, and R. de Tourreil, Phys. Rev. **C21**, 861 (1980).

[32] M. H. Partovi, and E. L. Lomon, Phys. Rev. **D2**, 1999 (1970); **D5**, 1192 (1972).

[33] R. Machleidt, K. Holinde, and C. Elster, Phys. Rep. **149**, 1 (1987).

[34] H. C. Kim, J. W. Durso, and K. Holinde, Phys. Rev. **C49**, 2355 (1994).

[35] G. Janssen, K. Holinde, and J. Speth, Phys. Rev. **C54**, 2218 (1996).

[36] V. G. J. Stoks, R. A. M. Klomp, M. C. M. Rentmeester, and J. J. de Swart, Phys. Rev. **C48**, 792 (1993).

[37] V. G. J. Stoks, R. A. M. Klomp, C. P. F. Terheggen, and J. J. de Swart, Phys. Rev. C **49**, 2950 (1994).

[38] R. B. Wiringa, V. G. J. Stoks, and R. Schiavilla, Phys. Rev. **C51**, 38 (1995).

[39] R. Machleidt, F. Sammarruca, and Y. Song, Phys. Rev. **C53**, 1483 (1996); R. Machleidt, Phys. Rev. **C63**, 024001 (2001).

[40] W. Glöckle, H. Witala, D. Hüber, H. Kamada, and J. Golak, Phys. Rep. **274**, 107 (1996).

[41] R. Machleidt and D. R. Entem. Phys. Rep. **503**, 1 (2011).

[42] K. Orginos, A. Parreño, M. J. Savage, S. R. Beane, E. Chang, and W. Detmold, Phys. Rev. D **92**, 114512 (2015).

[43] T. Hatsuda, J. Phys. Conf. Ser. **381**, 012020 (2012).

[44] S. Weinberg, Physica **96A**, 327 (1979).

[45] S. Weinberg, Phys. Lett. **B251**, 288 (1990).

[46] S. Weinberg, Phys. Lett. **B295**, 114 (1992).

[47] N. Kaiser, R. Brockmann, and W. Weise, Nucl. Phys. **A625**, 758 (1997).

[48] D. R. Entem, N. Kaiser, R. Machleidt, and Y. Nosyk, Phys. Rev. C **91**, 014002 (2015).

[49] D. R. Entem, N. Kaiser, R. Machleidt, and Y. Nosyk, Phys. Rev. C **92**, 064001 (2015).

[50] R. Machleidt. Int. J. Mod. Phys. **E26**, 1740018 (2017).

[51] H. W. Hammer, S. König, and U. van Kolck, Rev. Mod. Phys. **92**, 025004 (2020).

[52] R. Machleidt and F. Sammarruca, Eur. Phys. J. A **56**, 95 (2020).

[53] E. Epelbaum, H.-W. Hammer and U.-G. Meißner, Rev. Mod. Phys. **81**, 1773 (2009).

[54] S. Coleman, J. Wess and B. Zumino, Phys. Rev. **177**, 2239 (1969); C.G. Callan, S. Coleman, J. Wess and B. Zumino, Phys. Rev. **177**, 2247 (1969).

[55] H. Krebs, A. Gasparyan, and E. Epelbaum, Phys. Rev. C **85**, 054006 (2012).

[56] D. R. Entem, R. Machleidt, and Y. Nosyk, Phys. Rev. C **96**, 024004 (2017).

[57] K. A. Olive *et al.* (Particle Data Group), Chin. Phys. C **38**, 090001 (2014).

[58] N. Kaiser, Phys. Rev. C**64**, 057001 (2001).

[59] N. Kaiser, Phys. Rev. C**61**, 014003 (1999).

[60] N. Kaiser, Phys. Rev. C**62**, 024001 (2000).

[61] R. Blankenbecler and R. Sugar, Phys. Rev. **142**, 1051 (1966).

[62] B. D. Carlesson et al., Phys. Rev. X **6**, 011019 (2016).

[63] P. Reinert, H. Krebs and E. Epelbaum, Eur. Phys. J. A **54**, 86 (2018).

[64] A. Ekström, G. Hagen, T. D. Morris, T. Papenbrock and P.D. Schwartz, Phys. Rev. C **97**, 024332 (2018).

[65] E. Epelbaum, H. Krebs, and Ulf-G. Meibner, Eur. Phys. J. A**51**, 53 (2015).

[66] R. A. Arndt, W. J. Briscoe, I.I.Strakovsky, and R. L. Workman, Phys. Rev. **C76**, 025209 (2007).

[67] M. Hoferichter, J. Ruiz de Elvira, B. Kubis, and U.-G. Meißner, Phys. Rev. Lett. **115**, 192301 (2015); Phys. Rep. **625**, 1 (2016).

[68] R. Machleidt, Phys. Rev. C**63**, 024001 (2001)